Time-consistent hopping transport with vibration-mode-resolved electron-phonon couplings

Sebastian Hutsch, Michel Panhans, and Frank Ortmann
Department of Chemistry, Technische Universität München, 85748 Garching b. München, Germany
and Center for Advancing Electronics Dresden, Technische Universität Dresden, 01062 Dresden, Germany

(Received 4 April 2021; revised 5 August 2021; accepted 9 August 2021; published 25 August 2021)

Charge transport in organic semiconductors is affected by the complex interaction between charge carriers and molecular vibrations. A common way to treat the molecular vibrations in hopping approaches is by condensing them into a single analytical parameter, the reorganization energy. In contrast, here we present a nonadiabatic hopping transport approach that avoids this approximation by dividing the vibrational spectrum of organic molecules into three distinct analytical classes, namely the quasistatic, low-frequency dynamic, and high-frequency dynamic modes. The quasistatic and dynamic regimes are separated time consistently with respect to the timescale of the hopping events, which results in charge transfer events driven by a set of strongly coupling driving modes. Using these time-consistent hopping rates, we compute the charge carrier mobilities for a set of hopping transport materials and a control set of band-transport materials and compare them to experimental values. The resulting mobilities are consistent for both sets by showing similar values for the hopping transport materials and lower values for the control set of band-transport materials due to the absence of coherent transport contributions. We further study other popular hopping approaches such as the Marcus theory and the Levich-Jortner theory and observe substantial inconsistencies for them.

DOI: 10.1103/PhysRevB.104.054306

I. INTRODUCTION

Organic semiconductors enable electronic devices such as organic light emitting diodes, organic photovoltaic cells, and organic transistors, all of which rely on charge-transfer (CT) and charge-transport processes [1–12]. The theoretical description of these processes in molecular systems is intensively discussed. Various aspects of electronic transport are debated [13–23] and it remains a challenge to predict the charge carrier mobility even in well-defined systems such as molecular crystals while treating the molecular vibrations physically consistent. The main reason is that the vibrational modes that affect the electronic properties are distributed over a large range of vibration frequencies even for small molecules [24,25].

To deal with such complexity, elaborate approaches have been proposed [22,26–30], where the vibrations are usually treated either dynamically in polaron theories [31–33] or quasistatically, such as in transient localization theory [34,35]. These simplifications enable the calculation of the charge carrier mobility using approximate phonons at a large scale [36]. Also polaron hopping models can efficiently deal with a large number of structures and are widely used [15,37–40]. They have the advantage of being applicable to not only crystalline systems, but also disordered systems (such as polycrystalline ones or blends) due to their low computational demands. These charge transport theories usually fall into two categories, namely adiabatic approaches [41,42] and nonadiabatic approaches, such as the Marcus hopping (MH) theory [43,44]. In these approaches the complex interplay of electrons and molecular vibrations is approximated by collecting all vibrational modes into a single parameter, the reorganization energy Λ. However, given that the vibrational spectrum of organic semiconductors covers several orders of magnitude in mode energy (see Fig. 1), the significance of the full reorganization energy Λ is questionable and it should be avoided [45,46]. An improvement is performed in the Levich-Jortner hopping (LJH) theory [47], where, in the original form, intramolecular high-frequency modes and environmental fluctuations are distinguished and treated differently. Another improvement is achieved by a fully quantum mechanical treatment of molecular vibrations [29,48]. Despite these improvements, polaron hopping approaches commonly treat the intramolecular vibrations *dynamically*. However, a dynamical treatment of the slowest molecular vibrations becomes inappropriate for elevated hopping rates, which leads to a self-consistency problem for the hopping time [49,50].

In this work we study a time-consistent hopping (TCH) approach based on the Kubo formalism and avoid Fermi's golden rule, which allows separating the molecular vibrations into slow quasistatic and fast dynamic modes. The latter are further split into low-frequency and high-frequency modes in the spirit of LJH to obtain a hopping rate that is numerically easy to process without loss in accuracy. Based on the time-consistent separation of quasistatic and dynamic modes (see, e.g., the intramolecular vibrational spectrum in Fig. 1 for the molecule NTMTI), we find that the charge transfer is driven by strongly coupling *driving* modes, analogous to cases described by adiabatic approaches [41,42], but here obtained by a fully quantum-mechanical treatment of the molecular vibrations. When the TCH approach is applied to crystalline organic semiconductors with moderate mobility, for which

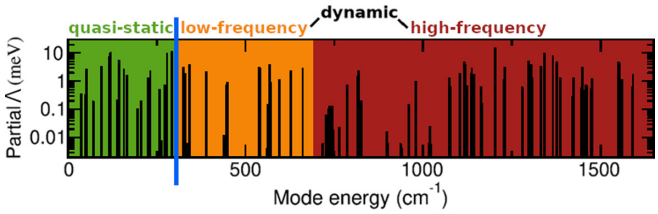

FIG. 1. Exemplary separation of the intramolecular vibrations in the TCH approach based on the spectral distribution of the vibration-mode-resolved reorganization energy of NTMTI.

the conditions for nonadiabatic hopping (e.g., the limit of narrow electronic bands) are estimated to be valid, it quantitatively reproduces experimental mobilities. When applied to a reference set of high-mobility organic crystals, for which the hopping limit is *not* valid and transport occurs via more delocalized states, the TCH approach yields mobilities that are systematically lower than experimental mobilities, since it describes only the incoherent hopping contribution to transport. Finally, the widely used MH and LJH theories are analyzed, which reveals that both theories violate time consistency.

II. DERIVATION OF THE HOPPING RATE EXPRESSION

A. Theoretical framework

We first present the derivation of the hopping approach within the Kubo formalism and the mode separation into quasistatic and dynamic modes. In the Kubo formalism the charge carrier mobility in transport direction reads [51–53]

$$\mu = \frac{1}{N_0 e_0}\frac{1}{2k_\mathrm{B}T}\int_{-\infty}^{\infty} dt\,\langle j(t)j(0)\rangle_H, \tag{1}$$

where the brackets are defined as $\langle A\rangle_H = \mathrm{Tr}[\rho A]$ with the equilibrium density operator ρ and $j(t) = e^{\frac{itH}{\hbar}} j e^{-\frac{itH}{\hbar}}$. N_0 is the carrier density, k_B is the Boltzmann constant, e_0 is the elementary charge, and T is the absolute temperature. Equation (1) is evaluated for the Holstein-Hamiltonian [31,52],

$$\begin{aligned} H &= H_\mathrm{el} + H_\mathrm{ph} + H_\text{el-ph} \\ &= \sum_{MN}\varepsilon_{MN}a_M^\dagger a_N + \sum_\lambda \hbar\omega_\lambda\left(b_\lambda^\dagger b_\lambda + \frac{1}{2}\right) \\ &\quad + \sum_M\sum_\lambda \hbar\omega_\lambda g_M^\lambda (b_\lambda^\dagger + b_\lambda)a_M^\dagger a_M. \end{aligned} \tag{2}$$

It uses a molecular site representation with on-site energies $\varepsilon_{MM} \equiv \varepsilon_M$ and transfer integrals ε_{MN}. The linear, local electron-phonon coupling constant g_M^λ describes the coupling of mode λ to the electron at site M. The restriction to linear electron-phonon coupling is a good approximation for typical organic semiconductors [54]. Albeit nonlocal couplings (the coupling of the molecular vibrations to the transfer integrals) can take an active localizing role in systems with delocalized charge carriers [16,55], for materials in the hopping regime with large local couplings and small transfer integrals they tend to give rise to only minor corrections [23]. Thus, the restriction to local coupling does not change the qualitative findings of this work, while significantly reducing the computational and analytical load.

Using the expression $j = \frac{e_0}{i\hbar}\sum_M [R_M a_M^\dagger a_M, H]$ for the current operator yields the correlation function

$$\begin{aligned} F &= \int_{-\infty}^{\infty} dt \left(\frac{e_0}{i\hbar}\right)^2 \sum_{MNKL} \varepsilon_{MN}\varepsilon_{KL}R_{KL}R_{MN}\frac{\theta}{Z}, \\ \theta &= \langle e^{-\beta H}e^{\kappa H}a_M^\dagger a_N e^{-\kappa H}a_K^\dagger a_L\rangle, \\ Z &= \langle e^{-\beta H}\rangle, \end{aligned} \tag{3}$$

with $\beta = 1/(k_\mathrm{B}T)$ being the inverse temperature. For reasons of brevity of notation, we use the abbreviation $\kappa = \frac{it}{\hbar}$ in the time evolution. The angular brackets denote the trace over electrons and all vibrations in the considered electron-phonon product spaces. A common way to treat the entanglement of the electronic and the vibrational degrees of freedom in θ stemming from Eq. (2) is to perform the Lang-Firsov transformation [56] with $A \to \tilde{A} = e^S A e^{S^\dagger}$, $S = \sum_M C_M a_M^\dagger a_M$, and $C_M = \sum_\lambda g_M^\lambda (b_\lambda^\dagger - b_\lambda)$. This transformation is the usual starting point for polaron theories, in which molecular vibrations are treated dynamically. Following the idea to separate the modes into different frequency regimes, the transformation includes only the fast, dynamic modes (dyn): $S = \sum_M \sum_\lambda^\mathrm{dyn} g_M^\lambda (b_\lambda^\dagger - b_\lambda)a_M^\dagger a_M$ in the following. In contrast, for slow modes, the charge carriers (on a given site M) experience only a fraction of the vibration period and slow modes should be excluded from the transformation. Physical intuition would suggest to replace the vibration coordinate by a frozen displaced one [57]. For longer timescales, the dynamics of these modes may become relevant, which motivates the term quasistatic (qs) that is used in the following. To perform the aforementioned separation of the vibrations into the two frequency regimes, we formally split the sums over the vibrational modes in H_ph and $H_\text{el-ph}$ in Eq. (2). The phonon Hamiltonian, for example, reads

$$\begin{aligned} H_\mathrm{ph} &= H_\mathrm{ph}^\mathrm{qs} + H_\mathrm{ph}^\mathrm{dyn} \\ &= \sum_\lambda^\mathrm{qs} \hbar\omega_\lambda\left(b_\lambda^\dagger b_\lambda + \frac{1}{2}\right) + \sum_\lambda^\mathrm{dyn} \hbar\omega_\lambda\left(b_\lambda^\dagger b_\lambda + \frac{1}{2}\right). \end{aligned} \tag{4}$$

Using this notation, we define the quasistatic and dynamic phonon Hamiltonians as $H^\mathrm{qs} = H_\mathrm{ph}^\mathrm{qs} + H_\text{el-ph}^\mathrm{qs}$ and $H^\mathrm{dyn} = H_\mathrm{ph}^\mathrm{dyn} + H_\text{el-ph}^\mathrm{dyn}$ and rewrite the Holstein-Hamiltonian Eq. (2) as

$$H = H_\mathrm{el} + H^\mathrm{dyn} + H^\mathrm{qs}. \tag{5}$$

The precise cutoff frequency (inverse hopping time τ_hop) for the separation is subject to a time-consistency condition and will be addressed in Sec. III.

B. Evaluation of the quasistatic modes

We first consider the slow motion of the quasistatic modes. More precisely, we model a situation in which the quasistatic modes cannot generate quantum entanglement. We therefore use the short-time approximation

$$e^{\kappa(H_\mathrm{el}+H^\mathrm{dyn}+H^\mathrm{qs})} \approx e^{\kappa(H_\mathrm{el}+H^\mathrm{dyn})}e^{\kappa H_\text{el-ph}^\mathrm{qs}}e^{\kappa H_\mathrm{ph}^\mathrm{qs}} \tag{6}$$

by neglecting the commutators between the separated parts of the Hamiltonian, namely $[H_\text{el-ph}^\mathrm{qs}, H_\mathrm{ph}^\mathrm{qs}]$ and $[H_\mathrm{el}, H_\text{el-ph}^\mathrm{qs}]$ as well as higher-order nested commutators. For instance, the

neglected term that is quadratic in time in the exponent $\frac{1}{2}\kappa^2[H^{\rm qs}_{\rm el\text{-}ph}, H^{\rm qs}_{\rm ph}]$ is smaller than the linear-in-κ terms on the right of Eq. (6) for the considered timescale (the hopping time $\tau_{\rm hop}$) and the low-frequency quasistatic modes. The same argument applies to $\frac{1}{2}\kappa^2[H_{\rm el}, H^{\rm qs}_{\rm el\text{-}ph}]$ for small transfer integrals. Note that, at this point, the full electronic bandwidth is still contained in its entangled form with the high-frequency modes in $e^{\kappa(H_{\rm el}+H^{\rm dyn})}$, which will be discussed later. As a result of this approximation, the quasistatic phonon Hamiltonian $H^{\rm qs}_{\rm ph}$ eventually vanishes from the time evolution in Eq. (3), reflecting the quasistatic nature of these modes. With this separation, the time evolution of the electronic operators evaluate to

$$\begin{aligned} a^\dagger_M(\kappa) &\equiv e^{\kappa H} a^\dagger_M e^{-\kappa H} = \bar{a}^\dagger_M e^{\kappa \sum^{\rm qs}_\lambda \hbar\omega_\lambda g^\lambda_M (b^\dagger_\lambda + b_\lambda)}, \\ a_N(\kappa) &\equiv e^{\kappa H} a_N e^{-\kappa H} = e^{-\kappa \sum^{\rm qs}_\lambda \hbar\omega_\lambda g^\lambda_N (b^\dagger_\lambda + b_\lambda)} \bar{a}_N, \end{aligned} \tag{7}$$

where the short-hand notation

$$\bar{a}_N \equiv a_N(\kappa)_{\rm el,dyn} = e^{\kappa(H_{\rm el}+H^{\rm dyn})} a_N e^{-\kappa(H_{\rm el}+H^{\rm dyn})} \tag{8}$$

is used and indicates that the time evolution driven by $H_{\rm el} + H^{\rm dyn}$ has yet to be evaluated. By inserting the electronic operators of Eq. (7) into θ in Eq. (3), one obtains

$$\begin{aligned} \theta = \langle & e^{-\beta(H_{\rm el}+H^{\rm dyn})} e^{-\beta H^{\rm qs}} e^{\kappa \sum^{\rm qs}_\lambda \hbar\omega_\lambda g^\lambda_M (b^\dagger_\lambda + b_\lambda)} \\ & \times e^{-\kappa \sum^{\rm qs}_\lambda \hbar\omega_\lambda g^\lambda_N (b^\dagger_\lambda + b_\lambda)} \bar{a}^\dagger_M \bar{a}_N a^\dagger_K a_L \rangle. \end{aligned} \tag{9}$$

Here the statistical operator of the quasistatic modes $e^{-\beta H^{\rm qs}}$ is separated similar to the time evolution above by neglecting the commutator in $e^{\frac{1}{2}(-\beta)^2[H_{\rm el}, H^{\rm qs}_{\rm el\text{-}ph}]}$.

The thermal averages with respect to the quasistatic modes and dynamic modes plus electrons can now be evaluated separately, as expressed in the form

$$\theta = \left\langle e^{-\beta(H_{\rm el}+H^{\rm dyn})} \theta^{\rm qs}_{MN} \bar{a}^\dagger_M \bar{a}_N a^\dagger_K a_L \right\rangle_{\rm el,dyn}. \tag{10}$$

Here $\theta^{\rm qs}_{MN}$ is defined as the targeted thermal average over the quasistatic modes:

$$\begin{aligned} \theta^{\rm qs}_{MN} = \langle & e^{-\beta H^{\rm qs}} e^{\kappa \sum^{\rm qs}_\lambda \hbar\omega_\lambda g^\lambda_M (b^\dagger_\lambda + b_\lambda)} \\ & \times e^{-\kappa \sum^{\rm qs}_\lambda \hbar\omega_\lambda g^\lambda_N (b^\dagger_\lambda + b_\lambda)} \rangle_{\rm qs}. \end{aligned} \tag{11}$$

In the thermal average in Eq. (11) we employ (in full analogy to the time-evolution above) the decoupling $e^{-\beta H^{\rm qs}} = e^{-\beta(H^{\rm qs}_{\rm el\text{-}ph}+H^{\rm qs}_{\rm ph})} = e^{-\beta H^{\rm qs}_{\rm el\text{-}ph}} e^{-\beta H^{\rm qs}_{\rm ph}}$. Evaluation with Wick's theorem yields

$$\theta^{\rm qs}_{MN} = Z^{\rm qs} e^{\frac{1}{2}\sum^{\rm qs}_\lambda (1+2N_\lambda)\left(-\beta \sum_P \hbar\omega_\lambda g^\lambda_P a^\dagger_P a_P + \kappa\hbar\omega_\lambda g^\lambda_M - \kappa\hbar\omega_\lambda g^\lambda_N\right)^2}, \tag{12}$$

where $N_\lambda = (e^{\frac{\hbar\omega_\lambda}{k_{\rm B}T}} - 1)^{-1}$ is the Bose-Einstein distribution function for the mode λ and $Z^{\rm qs} = \langle e^{-\beta H^{\rm qs}_{\rm ph}} \rangle_{\rm qs}$. We now assume that every mode λ is located at a particular molecular site (say Q), for which the coupling constant g^λ_Q is finite and $g^\lambda_{P\neq Q}$ is zero. This allows us to disentangle the exponential functions in Eq. (12) with respect to different sites, since the emerging products of couplings to different sites vanishes $g^\lambda_Q g^\lambda_{P\neq Q} = 0$. We obtain

$$\begin{aligned} \theta^{\rm qs}_{MN} = Z^{\rm qs} & e^{\frac{1}{2}\sum^{\rm qs}_\lambda (1+2N_\lambda) \sum_{P\neq M,N} \left[-\beta\hbar\omega_\lambda g^\lambda_P a^\dagger_P a_P\right]^2} \\ & \times e^{\frac{1}{2}\sum^{\rm qs}_\lambda (1+2N_\lambda)\left[\left(\kappa - \beta a^\dagger_M a_M\right)\hbar\omega_\lambda g^\lambda_M\right]^2} \\ & \times e^{\frac{1}{2}\sum^{\rm qs}_\lambda (1+2N_\lambda)\left[\left(-\kappa - \beta a^\dagger_N a_N\right)\hbar\omega_\lambda g^\lambda_N\right]^2}. \end{aligned} \tag{13}$$

C. Description with random disorder

We continue with the observation that the exponentials of electron operators occurring in Eq. (13) can be written with a Gaussian random variable ξ^λ for each quasistatic mode λ according to

$$\begin{aligned} & e^{\frac{1}{2}\sum^{\rm qs}_\lambda (1+2N_\lambda)\left(\kappa - \beta a^\dagger_M a_M\right)^2 (\hbar\omega_\lambda g^\lambda_M)^2} \\ & \quad = \frac{1}{R}\sum_i^R e^{\left(\kappa - \beta a^\dagger_M a_M\right)\sum^{\rm qs}_\lambda (\hbar\omega_\lambda g^\lambda_M)\sqrt{(1+2N_\lambda)}\xi^\lambda_i}, \end{aligned} \tag{14}$$

where the index i runs over all possible configurations of the quasistatic modes (i.e., random values of ξ^λ_i) R. We remember from above that each vibrational mode couples to only one specific site. As a consequence, the set of modes λ coupling to site M and the set of modes λ' coupling to site N are described by independent Gaussian random values ξ^λ_i and $\xi^{\lambda'}_i$, yielding

$$\begin{aligned} & e^{\frac{1}{2}\sum^{\rm qs}_\lambda (1+2N_\lambda)\left[\left(\kappa - \beta a^\dagger_M a_M\right)\hbar\omega_\lambda g^\lambda_M\right]^2} \\ & \quad \times e^{\frac{1}{2}\sum^{\rm qs}_\lambda (1+2N_\lambda)\left[\left(-\kappa - \beta a^\dagger_N a_N\right)\hbar\omega_\lambda g^\lambda_N\right]^2} \\ & \quad = \frac{1}{R}\sum_i^R e^{\left(\kappa - \beta a^\dagger_M a_M\right)V_M(\boldsymbol{\xi}_i) + \left(-\kappa - \beta a^\dagger_N a_N\right)V_N(\boldsymbol{\xi}_i)}, \end{aligned} \tag{15}$$

with the short-hand notation

$$V_M(\boldsymbol{\xi}_i) = \sum_\lambda^{\rm qs} (\hbar\omega_\lambda g^\lambda_M)\sqrt{(1+2N_\lambda)}\xi^\lambda_i. \tag{16}$$

Here we have introduced $\boldsymbol{\xi}_i = (\xi^1_i, \ldots, \xi^{n_{\rm qs}}_i)$ as a vector notation for the set of all independent Gaussian random values ξ^λ_i generating the random configuration i. The same argument is applied to the remaining sites $P \neq M, N$ occurring in Eq. (13). For a specific configuration $\boldsymbol{\xi}_i$, $\theta^{\rm qs}_{MN}$ becomes

$$\begin{aligned} \theta^{\boldsymbol{\xi}_i}_{MN} = Z^{\rm qs} & e^{\left(\kappa - \beta a^\dagger_M a_M\right)V_M(\boldsymbol{\xi}_i) + \left(-\kappa - \beta a^\dagger_N a_N\right)V_N(\boldsymbol{\xi}_i)} \\ & \times e^{\sum_{P\neq M,N}(-\beta a^\dagger_P a_P)V_P(\boldsymbol{\xi}_i)}, \end{aligned} \tag{17}$$

where one has to keep in mind that an average over a sufficient number of realizations $\boldsymbol{\xi}_i$ has to be performed. We further abbreviate $\boldsymbol{\xi}_i$ as $\boldsymbol{\xi}$ and suppress the explicit dependence of V on $\boldsymbol{\xi}$ in the notation for readability. For a specific configuration $\boldsymbol{\xi}$, Eq. (10) becomes

$$\begin{aligned} \theta^{\boldsymbol{\xi}} = Z^{\rm qs} \langle & e^{-\beta(H_{\rm el}+H^{\rm dyn})} e^{\left(\kappa - \beta a^\dagger_M a_M\right)V_M - \left(\kappa + \beta a^\dagger_N a_N\right)V_N} \\ & \times e^{\sum_{P\neq M,N}\left(-\beta a^\dagger_P a_P\right)V_P} \bar{a}^\dagger_M \bar{a}_N a^\dagger_K a_L \rangle_{\rm el,dyn}. \end{aligned} \tag{18}$$

Since the new random disorder terms $e^{-\beta V_P a^\dagger_P a_P}$ are diagonal in the electronic operators, we define the new condensed statistical operator corresponding to the electronic on-site disorder $e^{-\beta H_{\rm dis}} = e^{-\beta \sum_P V_P a^\dagger_P a_P}$, which indicates that each electronic

site experiences an energetic shift caused by the quasistatic modes. By rearranging the terms we obtain

$$\theta^{\xi} = Z^{\mathrm{qs}} e^{\kappa \Delta E^{\mathrm{qs}}_{MN}} \langle e^{-\beta(H_{\mathrm{el}}+H^{\mathrm{dyn}})} e^{-\beta H_{\mathrm{dis}}} \bar{a}^{\dagger}_{M} \bar{a}_{N} a^{\dagger}_{K} a_{L} \rangle_{\mathrm{el,dyn}}, \quad (19)$$

with $\Delta E^{\mathrm{qs}}_{MN} \equiv V_M - V_N$. We now assume equal molecules on site M and N, that is for every mode λ coupling to site M with g^{λ}_{M} there is an equivalent mode λ' coupling to site N with $g^{\lambda'}_{N} = g^{\lambda}_{M}$. Thus, by utilizing the properties of Gaussian random variables the random energy difference $\Delta E^{\mathrm{qs}}_{MN}$ between sites M and N can finally be expressed by a random variable following a Gaussian distribution of variance

$$(\sigma^{\mathrm{qs}})^2 = \sum_{\lambda}^{\mathrm{qs}} 2\hbar^2 \omega_{\lambda}^2 (g^{\lambda}_{M})^2 (1 + 2N_{\lambda}). \quad (20)$$

D. Treatment of dynamic modes and electronic trace

We now carry out the remaining traces in Eq. (19). For moderate transfer integrals (which we consider for the TCH approach to be valid), a polaronic treatment of the dynamic modes is suitable. We therefore perform the Lang-Firsov transformation with the dynamic modes according to $A \rightarrow \tilde{A} = e^{S} A e^{S^{\dagger}}$ with $S = \sum^{\mathrm{dyn}}_{M,\lambda} g^{\lambda}_{M} (b^{\dagger}_{\lambda} - b_{\lambda}) a^{\dagger}_{M} a_{M}$ and obtain

$$\theta^{\xi} = Z^{\mathrm{qs}} e^{\kappa \Delta E^{\mathrm{qs}}_{MN}} \langle e^{-\beta(\tilde{H}_{\mathrm{el}}+\tilde{H}^{\mathrm{dyn}})} e^{-\beta H_{\mathrm{dis}}} \tilde{\bar{a}}^{\dagger}_{M} \tilde{\bar{a}}_{N} \tilde{a}^{\dagger}_{K} \tilde{a}_{L} \rangle_{\mathrm{el,dyn}}, \quad (21)$$

where $\tilde{H}^{\mathrm{dyn}} = H^{\mathrm{dyn}}_{\mathrm{ph}} + H^{\mathrm{dyn}}_{\mathrm{rel}}$ has been transformed into a form that separates electron and phonon operators. One obtains the particularly simple form

$$H^{\mathrm{dyn}}_{\mathrm{rel}} = -\sum^{\mathrm{dyn}}_{M,\lambda} (g^{\lambda}_{M})^2 \hbar \omega_{\lambda} a^{\dagger}_{M} a_{M} = -\sum_{M} \Lambda^{\mathrm{dyn}} a^{\dagger}_{M} a_{M}, \quad (22)$$

with the definition of the polaron shift $\Lambda^{\mathrm{dyn}} = \sum^{\mathrm{dyn}}_{\lambda} (g^{\lambda}_{M})^2 \hbar \omega_{\lambda}$ (assuming $g^{\lambda}_{M} = g^{\lambda'}_{N}$). The nondiagonal electronic Hamiltonian $H_{\mathrm{el}} = \sum_{MN} \varepsilon_{MN} a^{\dagger}_{M} a_{N}$ is transformed to

$$\tilde{H}_{\mathrm{el}} = \sum_{MN} a^{\dagger}_{M} e^{C_M} \varepsilon_{MN} e^{-C_N} a_{N}, \quad (23)$$

with $C_M = \sum^{\mathrm{dyn}}_{\lambda} g^{\lambda}_{M} (b^{\dagger}_{\lambda} - b_{\lambda})$. Considering that only the dynamic modes contribute to the Lang-Firsov transformation, the resulting renormalization of the electronic couplings ε_{MN} by C_M can be estimated by performing the trace over these modes:

$$\langle \tilde{H}_{\mathrm{el}} \rangle_{\mathrm{dyn}} = \sum_{M} \varepsilon_{M} a^{\dagger}_{M} a_{M} + \sum_{M \neq N} \tilde{\varepsilon}_{MN} a^{\dagger}_{M} a_{N},$$

$$\tilde{\varepsilon}_{MN} = \varepsilon_{MN} e^{-\sum^{\mathrm{dyn}}_{\lambda} (1+2N_{\lambda}) (g^{\lambda}_{M})^2}. \quad (24)$$

These fast dynamic modes therefore lead to a narrowing (reduction) of the transfer integrals to $\tilde{\varepsilon}_{MN}$. If the bare transfer integrals are small or if the narrowing of the transfer integrals due to the fast dynamic modes is significant (which is the application regime of the hopping approach), the energy $\tilde{\varepsilon}_{MN}$ is smaller than the other terms in the time evolution and statistical operator and will be neglected in the following ("narrow-band limit"). That is, we assume that the transfer integral is too small to cause a significant expansion of the wave packet before the actual hopping event driven by molecular vibrations takes place. The consistency of this approximation for the studied molecules will be discussed further below and in Appendix A. We define the resulting electronic Hamiltonian:

$$\tilde{H}'_{\mathrm{el}} = \langle \tilde{H}_{\mathrm{el}} \rangle_{\mathrm{dyn}} + H^{\mathrm{dyn}}_{\mathrm{rel}} = \sum_{M} (\varepsilon_{M} - \Lambda^{\mathrm{dyn}}) a^{\dagger}_{M} a_{M}, \quad (25)$$

which is diagonal in the electronic sites. With $\tilde{a}_{L} = e^{-C_L} a_{L}$ and $\tilde{a}^{\dagger}_{K} = a^{\dagger}_{K} e^{C_K}$ we can now evaluate the remaining time evolution of the electronic operators in Eq. (21):

$$\begin{aligned} \tilde{\bar{a}}_{N} &= e^{\kappa H^{\mathrm{dyn}}_{\mathrm{ph}}} e^{\kappa \tilde{H}'_{\mathrm{el}}} \tilde{a}_{N} e^{-\kappa \tilde{H}'_{\mathrm{el}}} e^{-\kappa H^{\mathrm{dyn}}_{\mathrm{ph}}} \\ &= e^{-\kappa(\varepsilon_N - \Lambda^{\mathrm{dyn}})} e^{-C_N(t)} a_{N}, \\ \tilde{\bar{a}}^{\dagger}_{M} &= a^{\dagger}_{M} e^{C_M(t)} e^{\kappa(\varepsilon_M - \Lambda^{\mathrm{dyn}})}, \end{aligned} \quad (26)$$

with $C_N(t) = \sum^{\mathrm{dyn}}_{\lambda} g^{\lambda}_{N} (b^{\dagger}_{\lambda} e^{i\omega_{\lambda} t} - b_{\lambda} e^{-i\omega_{\lambda} t})$. By collecting the results of the previous steps into Eq. (21) we obtain

$$\begin{aligned} \theta^{\xi} = Z^{\mathrm{qs}} e^{\kappa \Delta E^{\mathrm{qs}}_{MN}} \langle & e^{-\beta H^{\mathrm{dyn}}_{\mathrm{ph}}} e^{-\beta(\tilde{H}'_{\mathrm{el}} + H_{\mathrm{dis}})} e^{C_M(t)} e^{\kappa(\varepsilon_M - \Lambda^{\mathrm{dyn}})} \\ & \times e^{-\kappa(\varepsilon_N - \Lambda^{\mathrm{dyn}})} e^{-C_N(t)} e^{C_K} e^{-C_L} a^{\dagger}_{M} a_{N} a^{\dagger}_{K} a_{L} \rangle_{\mathrm{el,dyn}}. \end{aligned} \quad (27)$$

The energy difference generated by the quasistatic modes in $e^{\kappa \Delta E^{\mathrm{qs}}_{MN}}$ and the on-site energy difference in $e^{\kappa(\varepsilon_M - \varepsilon_N)}$ can be collected into a single exponential term $e^{\kappa \Delta \bar{E}_{MN}}$ with $\Delta \bar{E}_{MN} = (V_M - V_N) + (\varepsilon_M - \varepsilon_N)$, reflecting that the quasistatic disorder alters the on-site energies. In the same way we can condense the statistical operators $e^{-\beta \tilde{H}'_{\mathrm{el}}}$ and $e^{-\beta H_{\mathrm{dis}}}$ in a single statistical operator: $e^{-\beta \bar{H}_{\mathrm{el}}} = e^{-\beta \sum_M (\varepsilon_M - \Lambda^{\mathrm{dyn}} + V_M) a^{\dagger}_{M} a_{M}}$.

The trace over the electronic and dynamic phonon degrees of freedom can now be separated to arrive at

$$\begin{aligned} \theta^{\xi} = Z^{\mathrm{qs}} e^{\kappa \Delta \bar{E}_{MN}} & \langle e^{-\beta \bar{H}_{\mathrm{el}}} a^{\dagger}_{M} a_{N} a^{\dagger}_{K} a_{L} \rangle_{\mathrm{el}} \\ & \times \left\langle e^{-\beta H^{\mathrm{dyn}}_{\mathrm{ph}}} e^{C_M(t)} e^{-C_N(t)} e^{C_K} e^{-C_L} \right\rangle_{\mathrm{dyn}}. \end{aligned} \quad (28)$$

The electronic contribution is evaluated first to obtain

$$\begin{aligned} & \langle e^{-\beta \bar{H}_{\mathrm{el}}} a^{\dagger}_{M} a_{N} a^{\dagger}_{K} a_{L} \rangle_{\mathrm{el}} \\ & \quad = Z^{\mathrm{el}} [\delta_{MN} \delta_{KL} n_M n_K + \delta_{ML} \delta_{NK} n_M (1 - n_N)], \end{aligned} \quad (29)$$

with the Fermi-Dirac distribution function $n_M = [\exp(\frac{\varepsilon_M - \Lambda^{\mathrm{dyn}} + V_M}{k_{\mathrm{B}} T}) + 1]^{-1}$ and $Z^{\mathrm{el}} = \langle e^{-\beta \bar{H}_{\mathrm{el}}} \rangle_{\mathrm{el}}$. There the quasistatic modes affect the on-site energies ε_M by the energy shift V_M and the dynamic modes lead to the polaron shift Λ^{dyn}. We recall the geometric prefactors in the original expression Eq. (3) and find that only the second term in Eq. (29), which is proportional to $\propto \delta_{ML} \delta_{NK}$, contributes. The remaining trace over the dynamic phonons evaluates to [52]

$$\begin{aligned} & \left\langle e^{-\beta H^{\mathrm{dyn}}_{\mathrm{ph}}} e^{C_M(t)} e^{-C_N(t)} e^{C_K} e^{-C_L} \right\rangle_{\mathrm{dyn}} \delta_{ML} \delta_{NK} \\ & \quad = Z^{\mathrm{dyn}} e^{-2\phi(0)} e^{2\phi(t)} \delta_{ML} \delta_{NK}, \end{aligned} \quad (30)$$

with $\phi(t) = \sum^{\mathrm{dyn}}_{\lambda} (g^{\lambda}_{M})^2 [(N_{\lambda} + 1) e^{-i\omega_{\lambda} t} + N_{\lambda} e^{i\omega_{\lambda} t}]$ and $Z^{\mathrm{dyn}} = \langle e^{-\beta H^{\mathrm{dyn}}_{\mathrm{ph}}} \rangle_{\mathrm{dyn}}$. By collecting all terms we obtain

$$\begin{aligned} \theta^{\xi} &= Z^{\mathrm{dyn}} Z^{\mathrm{qs}} Z^{\mathrm{el}} e^{\kappa \Delta \bar{E}_{MN}} e^{\phi^{\mathrm{dyn}}(t)} \delta_{ML} \delta_{NK} n_M (1 - n_N), \\ \phi^{\mathrm{dyn}}(t) &= -2\phi(0) + 2\phi(t). \end{aligned} \quad (31)$$

Note that, when calculating the correlation function F using Eq. (3), the first three terms $Z^{\mathrm{dyn}} Z^{\mathrm{qs}} Z^{\mathrm{el}}$ in Eq. (31) cancel with

the partition function Z in Eq. (3), which is evaluated to $Z = Z^{\mathrm{dyn}}Z^{\mathrm{qs}}Z^{\mathrm{el}} = \langle e^{-\beta H_{\mathrm{ph}}^{\mathrm{dyn}}}\rangle_{\mathrm{dyn}}\langle e^{-\beta H_{\mathrm{ph}}^{\mathrm{qs}}}\rangle_{\mathrm{qs}}\langle e^{-\beta \bar{H}_{\mathrm{el}}}\rangle_{\mathrm{el}}$ by applying the aforementioned transformations in an analogous fashion. This gives the final correlation function

$$F = \left(\frac{e_0}{\hbar}\right)^2 \sum_{MN} \varepsilon_{MN}^2 R_{MN}^2 n_M (1-n_N)\bar{F}(\Delta\bar{E}_{MN}),$$

$$\bar{F}(\Delta\bar{E}_{MN}) = \int_{-\infty}^{\infty} dt\, e^{it\Delta\bar{E}_{MN}/\hbar} e^{\phi^{\mathrm{dyn}}(t)}, \tag{32}$$

with the Fourier transform $\bar{F}(\Delta\bar{E}_{MN})$ at the argument of the on-site energy difference $\Delta\bar{E}_{MN} = \Delta E_{MN} + \Delta E_{MN}^{\mathrm{qs}}$, whereby $\Delta E_{MN}^{\mathrm{qs}}$ realizes the potential shifts due to the quasistatic modes and follows the Gaussian distribution defined by Eq. (20).

Inserting Eq. (32) into Eq. (1) and considering a single charge carrier (low density limit) in the hopping process, we obtain the mobility in transport direction α:

$$\mu_\alpha = \frac{e_0}{\hbar^2}\frac{1}{2k_{\mathrm{B}}T}\sum_{MN}\varepsilon_{MN}^2 R_{MN\alpha}^2 \bar{F}(\Delta\bar{E}_{MN}). \tag{33}$$

Utilizing the Einstein-Smoluchowski relation [58,59] $\mu_\alpha = \frac{e_0 D_\alpha}{k_{\mathrm{B}}T}$ and identifying the diffusion constant as $D_\alpha = \frac{\langle x_\alpha^2\rangle}{2t} = \frac{1}{2}\sum_{MN} R_{MN\alpha}^2 \nu_{MN}$, we finally obtain the expression for the hopping rate ν_{MN}:

$$\begin{aligned}
\nu_{MN}(\Delta E_{MN}) &= \frac{\varepsilon_{MN}^2}{\hbar^2}\int_{-\infty}^{\infty} dt\, e^{\frac{it}{\hbar}(\Delta E_{MN}+\Delta E_{MN}^{\mathrm{qs}})} e^{\phi^{\mathrm{dyn}}(t)},\\
\phi^{\mathrm{dyn}}(t) &= -2\sum_{\lambda}^{\mathrm{dyn}} (g_M^\lambda)^2(2N_\lambda+1)\\
&\quad + 2\sum_{\lambda}^{\mathrm{dyn}} (g_M^\lambda)^2(N_\lambda+1)e^{-i\omega_\lambda t}\\
&\quad + 2\sum_{\lambda}^{\mathrm{dyn}} (g_M^\lambda)^2 N_\lambda e^{i\omega_\lambda t}.
\end{aligned} \tag{34}$$

Equation (34) is the central hopping rate obtained from linear-response theory, which generalizes structurally similar hopping rates derived previously from perturbation theory [29,47,48,60] by including quasistatic intramolecular modes in $\Delta E_{MN}^{\mathrm{qs}}$ additionally to the dynamic modes in $\phi^{\mathrm{dyn}}(t)$.

E. Analytic separation of the dynamic modes into low-frequency and high-frequency modes

In order to simplify the analytic expressions, the time integration in Eq. (34) is calculated in the spirit of Levich-Jortner theory [47] by a separation of the dynamic modes into low-frequency (lf) and high-frequency (hf) dynamic modes. This is a reasonable approximation for the vibrational spectrum of organic molecules as shown in Appendix B. By means of the convolution theorem, one can distinguish the contributions of the low-frequency and high-frequency dynamic modes in

$$F(\Delta\bar{E}_{MN}) = \int_{-\infty}^{\infty} dt\, e^{it\Delta\bar{E}_{MN}/\hbar} e^{\phi^{\mathrm{dyn}}(t)} \tag{35}$$

according to

$$F(\Delta\bar{E}_{MN}) = \frac{1}{\hbar}\int_{-\infty}^{\infty} d\zeta\, F^{\mathrm{lf}}(\Delta\bar{E}_{MN}+\zeta)F^{\mathrm{hf}}(-\zeta). \tag{36}$$

The terms F^{lf} and F^{hf} are defined in full analogy to Eq. (35), but with sums in $\phi^{\mathrm{dyn}}(t)$ that are restricted to the respective class of modes, i.e.,

$$\begin{aligned}
F^{\mathrm{hf}}(-\zeta) &= \int_{-\infty}^{\infty} dt\, e^{-it\zeta/\hbar} e^{\phi^{\mathrm{hf}}(t)},\\
\phi^{\mathrm{hf}}(t) &= -2\sum_{\lambda}^{\mathrm{hf}} (g_M^\lambda)^2(2N_\lambda+1)\\
&\quad + 2\sum_{\lambda}^{\mathrm{hf}} (g_M^\lambda)^2(N_\lambda+1)e^{-i\omega_\lambda t}\\
&\quad + 2\sum_{\lambda}^{\mathrm{hf}} (g_M^\lambda)^2 N_\lambda e^{i\omega_\lambda t}.
\end{aligned} \tag{37}$$

The high-frequency dynamic modes are periodic at the considered timescales and show a vanishing occupation N_λ at room temperature. They are gathered into an effective mode of energy $\hbar\omega_{\mathrm{eff}} = \frac{2\sum_\lambda (g_M^\lambda)^2\hbar\omega_\lambda}{S_{\mathrm{eff}}}$ and coupling strength $S_{\mathrm{eff}} = 2\sum_\lambda (g_M^\lambda)^2$, which leads to the analytical expression

$$F^{\mathrm{hf}}(-\zeta) = e^{-S_{\mathrm{eff}}}\sum_k \frac{h}{k!} S_{\mathrm{eff}}^k \delta(\zeta + k\hbar\omega_{\mathrm{eff}}). \tag{38}$$

The low-frequency dynamic modes gathered in F^{lf} do not oscillate through a full period during the considered timescales and we thus apply the short-time approximation [60]. In this limit, the expansion of the exponential functions in $\phi^{\mathrm{lf}}(t)$ up to the quadratic order in t yields

$$F^{\mathrm{lf}}(\Delta\bar{E}+\zeta) = \sqrt{\frac{2\pi}{D^{\mathrm{lf}}}}\exp\left(\frac{-(\Delta\bar{E}+\zeta-\Lambda_{\mathrm{red}})^2}{2D^{\mathrm{lf}}\hbar^2}\right). \tag{39}$$

Here we introduce the *reduced reorganization energy* [45] $\Lambda_{\mathrm{red}} = 2\sum_\lambda^{\mathrm{lf}} (g_M^\lambda)^2\hbar\omega_\lambda$, which is obtained by summing only over the low-frequency dynamic modes. Accordingly, the width of the Gaussian in Eq. (39) depends only on these low-frequency dynamic modes and is defined as $D^{\mathrm{lf}} = 2\sum_\lambda^{\mathrm{lf}} (g_M^\lambda)^2\omega_\lambda^2(2N_\lambda+1)$. By introducing the reduced *thermal* reorganization energy $\Lambda_{\mathrm{th}}(T) = \frac{D^{\mathrm{lf}}(T)\hbar^2}{2k_{\mathrm{B}}T}$, the final hopping rate, which is used for the TCH approach, reads

$$\begin{aligned}
\nu_{MN} &= \frac{\sqrt{\pi}\varepsilon_{MN}^2 e^{-S_{\mathrm{eff}}}}{\hbar\sqrt{\Lambda_{\mathrm{th}}(T)k_{\mathrm{B}}T}}\sum_{k=0}^{\infty}\frac{(S_{\mathrm{eff}})^k}{k!}\\
&\quad\times\exp\left[\frac{-\left(\Delta E_{MN}^{\mathrm{qs}}-\Lambda_{\mathrm{red}}-k\hbar\omega_{\mathrm{eff}}\right)^2}{4\Lambda_{\mathrm{th}}(T)k_{\mathrm{B}}T}\right].
\end{aligned} \tag{40}$$

The low-frequency dynamic modes contribute to the reduced reorganization energy [45] $\Lambda_{\mathrm{red}} = 2\sum_\lambda^{\mathrm{lf}}\hbar\omega_\lambda (g_M^\lambda)^2$ and to the temperature-dependent thermal broadening $\Lambda_{\mathrm{th}}(T) = \sum_\lambda^{\mathrm{lf}}(\hbar\omega_\lambda)^2(g_M^\lambda)^2(2N_\lambda+1)/(k_{\mathrm{B}}T)$. The high-frequency modes contribute to an effective high-frequency mode of energy $\hbar\omega_{\mathrm{eff}} = \sum_\lambda^{\mathrm{hf}}\hbar\omega_\lambda (g_M^\lambda)^2 / \sum_\lambda^{\mathrm{hf}}(g_M^\lambda)^2$ and

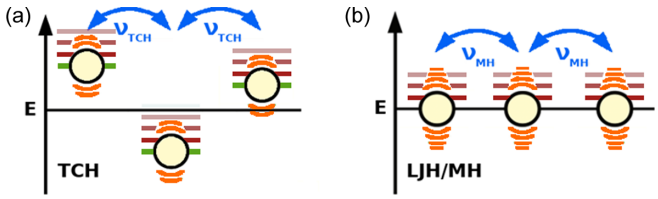

FIG. 2. Schematic comparison of the impact of the intramolecular modes on the energetics of the molecular sites in the TCH approach (a) and LJH/MH approach (b) using the color scale for the different modes from Fig. 1.

effective coupling $S_{\text{eff}} = 2\sum_{\lambda}^{\text{hf}}(g_M^{\lambda})^2$. Standard LJH theory can be obtained from Eq. (40) by applying the high-temperature limit to $\Lambda_{\text{th}}(T) \xrightarrow{T\to\infty} \Lambda_{\text{red}}$. This limit however does not need to be assumed and we use the expression $\Lambda_{\text{th}}(T)$. We therefore term Eq. (40) modified Levich-Jortner hopping (mLJH) rate.

The impact of the three frequency regimes on the hopping rate is illustrated in Fig. 2 for three sites. In TCH (left), the *quasistatic* modes generate static disorder in the electronic energies (green levels). On each side, the *low-frequency dynamic* modes generate an energetic broadening (orange) and the periodic *high-frequency dynamic* modes create phonon replica (red level sequence). Standard Marcus and Levich-Jortner theory (Fig. 2 right) only consider the presence of a single or two intramolecular dynamic frequency regimes, respectively.

III. REALIZATION OF TIME CONSISTENCY AND PHYSICAL INTERPRETATION

The TCH approach is based on the distinction between the quasistatic modes, which in general impede transport and dynamic modes, which in general enhance transport in the presence of static disorder. The mode separation depends on the timescale of charge transport, which in the case of hopping is the residence time $\tau_{\text{hop}} = 1/\nu_{MN}$ of the charge carrier. In turn, the residence time depends on the mode separation due to the different impact of the quasistatic and dynamic modes on the hopping rate ν_{MN} in Eq. (40). The resulting dependencies, which can be also observed in a similar fashion in other contexts [49,50], are visualized in Fig. 3(a). A consistent solution is obtained via a self-consistent or, more specifically, time-consistent algorithm. To this end, we define the dynamic modes as the modes that can pass through at least half of their vibration period τ^{dyn} during the residence time τ_{hop}, allowing them to explore their full conformation space during that time. Consequently, their frequency $\nu^{\text{dyn}} = 1/\tau^{\text{dyn}}$ should be larger than half the hopping rate ($2\nu_{\lambda}^{\text{dyn}} \geqslant 2\nu_{\text{min}}^{\text{dyn}} > \nu_{MN}$). All modes that are slower ($2\nu_{\lambda}^{\text{qs}} \leqslant 2\nu_{\text{max}}^{\text{qs}} \leqslant \nu_{MN}$) are treated quasistatically. This leads to the time-consistency (TC) condition between hopping rate and mode frequencies:

$$2\nu_{\text{max}}^{\text{qs}} \leqslant \nu_{\text{TCH}} < 2\nu_{\text{min}}^{\text{dyn}}. \tag{41}$$

The TCH rates ν_{TCH} are calculated individually for each hopping event. To realize Eq. (41), the hopping rate is calculated iteratively for each event as exemplary shown in Fig. 3(b).

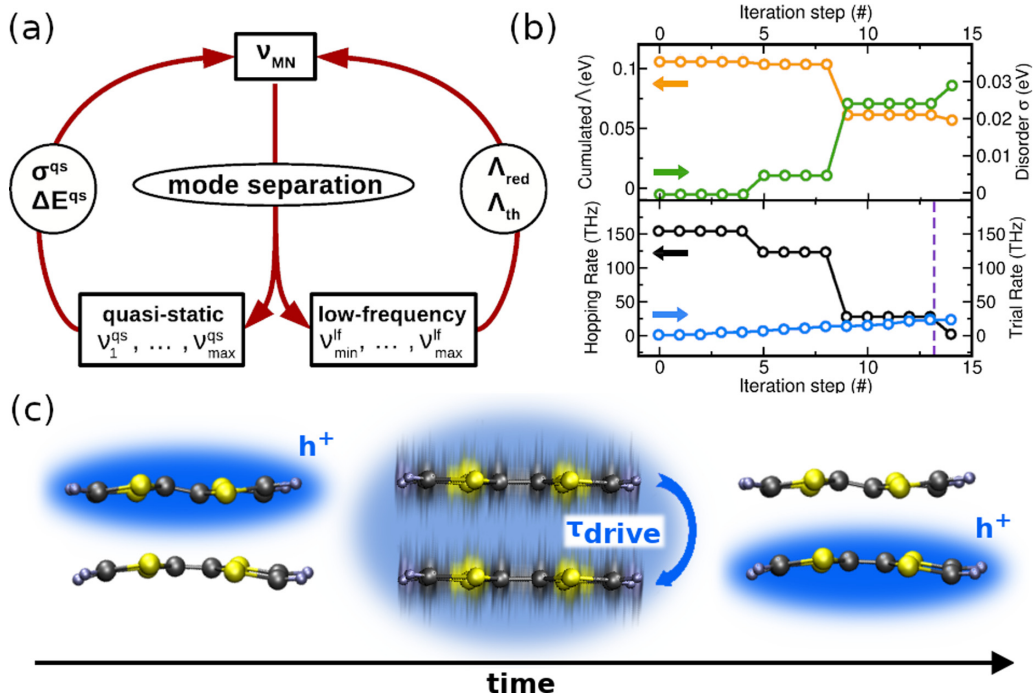

FIG. 3. Time-consistent hopping. (a) Schematic representation of the mutual dependencies: the hopping rate ν_{MN} depends on the particular separation of modes through the quantities (ΔE^{qs}, σ^{qs}, Λ_{th}, Λ_{red}). The separation of the modes in turn depends on the hopping rate. (b) Example of the iterative determination of the transport parameters for a single hopping event. Displayed are the preliminary transport parameters at each iteration step. Top panel: Dynamic reorganization energy (orange) and static disorder strength (green). Lower panel: Hopping rate (black) and current trial rate (blue). The last iteration determines ν_{TCH}. Lines are guide to the eye. (c) As a consequence of the time-consistent treatment, the CT is mainly driven by a set of strongly coupled driving modes and the CT takes place on the timescale of these modes.

The figure shows the iterative change of the transport parameters, hopping rates ν_{MN}, and *trial rate* $2\nu_{\max}^{\mathrm{qs}}$ of the fastest quasistatic mode in a given iteration step, evolving towards convergence. As a starting point, all modes are treated dynamically, for which the dynamic reorganization energy Λ is maximal and the static disorder strength σ^{qs} is zero (top panel) as commonly used in standard Levich-Jortner approaches. The resulting hopping rate is usually too large (bottom panel) and still violates Eq. (41), which implies that a number of modes should be treated quasistatically instead. In the progress of the algorithm, the number of quasistatic modes is gradually increased up to the time-consistency point fulfilling Eq. (41) [violet dashed line in the bottom panel of Fig. 3(b)]. Note that because the hopping rate (and thus the mode separation) depends on the random configurations $\boldsymbol{\xi}$ of the slowest modes, it may be that vibrations are quasistatic in one hopping event and dynamic in another.

The physical picture emerging from the time-consistency considerations is illustrated in Fig. 3(c) and is explained as follows. The hopping rate ν_{TCH} that fulfills the time-consistency condition Eq. (41) is eventually pinned at $\nu_{\mathrm{TCH}} = 2\nu^{\mathrm{drive}}$. One finds that ν^{drive} is the frequency of one of the strongly coupled *driving modes* of the system.

On its way towards the consistency point, there can be two inconsistency situations. In the case that these driving modes are part of the dynamic modes, one obtains too fast hopping rates ($\nu_{\mathrm{MN}} > 2\nu^{\mathrm{drive}}$) that are inconsistent with Eq. (41). In the opposite case that these driving modes belong to the set of quasistatic modes, one obtains too slow hopping rates ($\nu_{\mathrm{MN}} < 2\nu^{\mathrm{drive}}$) that are again inconsistent. The hopping event thus has to be driven by the emerging dynamics of the driving modes as illustrated in Fig. 3(c). For short times [left in Fig. 3(c)], the driving modes are frozen in a random quasistatic configuration. The resulting energetic disorder impedes transport and localizes the charge carrier on a single molecule. For longer times, the dynamics of the driving modes set in and enables the transfer of the charge (middle). For a short time interval directly after the transfer, the driving modes are again frozen and localize the charge carrier (right). Consequently, the CT takes place concertedly with the driving modes, it is driven by their motion. This finding also corroborates models such as the adiabatic limit of transition state theory [41,42].

IV. SELECTION AND CLASSIFICATION OF SYSTEMS

To study the characteristics of the derived TCH approach and compare it to other hopping theories, we choose 10 different molecular crystals with varying characteristics (see Fig. 4). They are selected to represent two prototypical regimes of transport in molecular crystals: hopping (localized) transport and bandlike (delocalized) transport. We consider five low-mobility materials ($\mu_{\mathrm{exp}} \lessapprox 1\ \mathrm{cm^2\,V^{-1}\,s^{-1}}$) that are classified in the localized hopping-transport regime (LOC, shown in green) at room temperature, which are NTMTI, TTF, DT-TTF, PMSB, and naphthalene. Five additional materials are classified into the delocalized transport regime (DEL, shown in violet) and are characterized by a high experimental charge carrier mobility ($\mu_{\mathrm{exp}} \approx 10\ \mathrm{cm^2\,V^{-1}\,s^{-1}}$), namely rubrene, pentacene, picene, DNTT, and DNBDT-C10. The rationale to include this second class of materials as a control

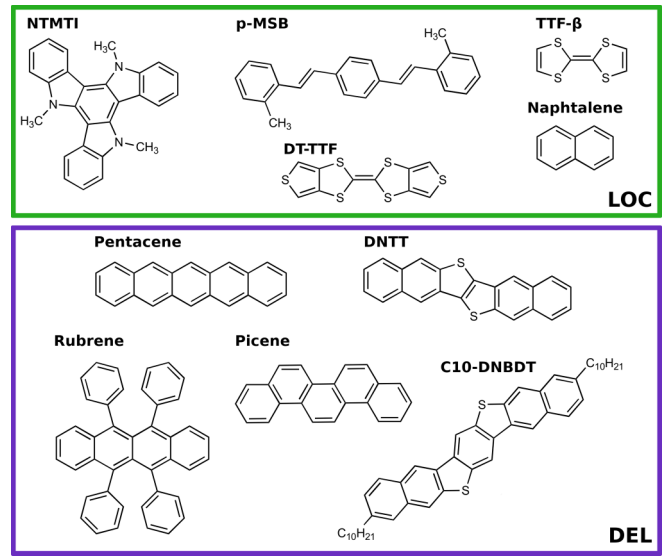

FIG. 4. Materials used to study the TCH and other nonadiabatic hopping approaches. The materials are classified into the hopping (localized) transport regime (LOC, green) and bandlike (delocalized) transport regime (DEL, violet).

set is that hopping approaches relying on narrow electronic bands should fail to reproduce the experimental mobility (if consistently employed) and predict lower mobilities due to the absence of coherent contributions.

The classification of the materials in one of the two transport regimes is performed based on the averaged degree of localization of the charge carrier on a single molecular site θ_{LOC}, which we estimate in a two-state model using *ab initio* material parameters. We therefore reduce the Holstein-Hamiltonian Eq. (2) to a purely electronic two-state Hamiltonian

$$H_{\text{two-state}} = \begin{pmatrix} 0 & \tilde{\varepsilon}_{12} \\ \tilde{\varepsilon}_{21} & (\varepsilon_2 - \varepsilon_1) \end{pmatrix}. \tag{42}$$

In the spirit of the TCH approach, the molecular vibrations enter in Eq. (42) in a separated fashion. The slow quasistatic modes generate disorder in the electronic on-site energies $(\varepsilon_2 - \varepsilon_1)$ following a Gaussian distribution according to Eq. (20). The fast dynamic modes generate a narrowing of the bare transfer integrals ε_{12} to $\tilde{\varepsilon}_{12}$ according to Eq. (24). The resulting eigenstates of the two-state Hamiltonian Eq. (42) allow us to draw conclusions on the degree of charge localization θ_{LOC} on a single molecular site caused by the interplay of the transfer integral and vibrational disorder. More details about the estimation and a comparison to a common estimation from transition-state theory [30] can be found in Appendix A.

The *ab initio* parameters entering the transport simulations and the estimation of the localization regime, such as the transfer integrals ε_{MN} and mode-resolved electron-phonon coupling g_M^{λ}, are calculated based on density functional theory (DFT). We used the B3LYP hybrid functional [61,62] in combination with the 6-311G** basis set [63,64] implemented in the Gaussian software package [65]. More details about the utilized methods, including the required computational costs, are summarized in Appendix C. The resulting *ab initio param-*

TABLE I. Studied molecules and relevant transport parameters as well as the estimators θ_{LOC} and θ_{HOP} and the final classification θ into the localized (LOC) and delocalized (DEL) transport regime. The references in the first column refer to the studied crystal structures. Λ_{tot} is the total reorganization energy used in Marcus theory. Λ_{red} is the reorganization energy excluding the high-energy modes that acts as an energy barrier in the TCH and mLJH approach. $\Lambda_{\mathrm{th}}(T)$ is the temperature-dependent reduced reorganization energy used in the thermal broadening in the TCH and mLJH approach. σ_{env} is the disorder parameter containing environmental disorder effects [66]. The values marked with * are estimated from comparison to known crystal structures.

Material	Λ_{tot} (meV)	Λ_{red} (meV)	$\Lambda_{\mathrm{th}}^{300\,\mathrm{K}}$ (meV)	ε_{MN} (meV)	σ_{env} (meV) [66]	θ_{LOC}	θ_{HOP}	θ	μ_{exp} ($\mathrm{cm}^2/\mathrm{V\,s}$)
TTF-β [67]	288	146	161	50	108	0.88	0.35	LOC	0.23 [68]
NTMTI [69]	226	120	107	31	71	0.88	0.27	LOC	0.37 [69]
PMSB [70]	408	248	282	44	90*	0.85	0.22	LOC	0.17 [71]
DT-TTF [72]	233	119	150	55	53	0.74	0.47	LOC	1.4 [73]
Naphthalene [74]	189	5	7	42	90	0.68	0.44	LOC	1.0 [75]
DNBDT-C10 [76]	89	30	39	49	75*	0.61	1.10	DEL	12.1 [76]
Picene [77]	190	43	48	79	82	0.58	0.83	DEL	9.0 [78]
DNTT [79]	134	40	35	98	75	0.46	1.46	DEL	8.3 [80]
Pentacene [81]	95	2	2	77	68	0.42	1.62	DEL	2.3 [82]
Rubrene [83]	160	48	51	104	53	0.41	1.30	DEL	15.4 [84]

eters and the experimental mobilities of the studied molecules are collected in Table I.

V. CHARGE-CARRIER MOBILITIES FROM TCH AND OTHER HOPPING APPROACHES

In order to realize variable configurations $\boldsymbol{\xi}$ of the quasistatic disorder, the hole mobilities of the studied crystals are simulated with a kinetic Monte Carlo scheme using the derived TCH rates and including environmental disorder effects [66]. More details about the simulations are presented in Appendix C. The resulting mobilities in the high-mobility directions are presented in Fig. 5(a) and are compared with experimental mobilities. To characterize the deviation between the mobilities of the two sets (in terms of their ratio $\mu^i_{\mathrm{calc}}/\mu^i_{\mathrm{exp}}$), we compute the geometric average $\Delta_{\mathrm{hop}} = \exp[\frac{1}{n}\sum_i^n \ln(\mu^i_{\mathrm{calc}}/\mu^i_{\mathrm{exp}})]$ over the $n = 5$ hopping materials, which would be one if both sets coincide. In Fig. 5(a) the TCH and the experimental mobilities correlate closely for the materials in the hopping regime (green dots) with $\Delta_{\mathrm{hop}} = 1.4$. For the control set of bandlike transport materials [violet dots in Fig. 5(a)], the TCH mobilities are about a factor of 10 below the experimental values. This quantifies that the hopping contributions are small for these systems as expected and indicates the dominance of coherent transport in the experiment, which is not captured by hopping approaches.

We use the TCH approach as a reference to study further hopping theories without time consistency such as the mLJH [Eq. (40)] and MH theory (with and without environmental disorder). The mobilities obtained with these models are visualized in Figs. 5(b)–5(d). To analyze the results, we further calculate the ratio between these hopping rates ν and the TCH rate ν_{TCH} for a multitude of hopping events in the main transport direction. The distributions of these ratios indicate the deviations from time consistency and are shown in Figs. 5(e)–5(h) for materials in the hopping regime (top panel) and bandlike regime (bottom panel). The average ratio $\overline{\nu/\nu_{\mathrm{TCH}}} = \exp[\frac{1}{n}\sum_i^n \ln(\nu^i/\nu^i_{\mathrm{TCH}})]$ is indicated in green (hopping) and violet (bandlike).

The mobilities calculated with the mLJH approach [Fig. 5(b)] are larger than the experimental values and TCH mobilities ($\Delta_{\mathrm{hop}} = 1.9$), which is traced back to the increased hopping rates shown in Fig. 5(f). The reason for this overestimation is found to be the missing time consistency, by which all modes are treated dynamically and enhance transport in the presence of environmental disorder. The only exception is pentacene, for which there are no strongly coupling low-frequency vibrations that could enhance the transport and thus their absence drastically reduces the mobility [inset in Fig. 5(b)]. Besides, the mLJH rates for the control set of bandlike materials are substantially increased compared to TCH as shown in Fig. 5(f). However, the resulting recovery of the experimental trend (except for pentacene) should be taken with caution, since it is an artifact of inconsistently treating also the slow intramolecular vibrations completely dynamically.

We next consider MH rates including static environmental disorder. The MH approach makes further approximations to the above mLJH theory by removing the distinction between low-frequency and high-frequency dynamic modes (i.e., $\Lambda_{\mathrm{red}} \to \Lambda_{\mathrm{tot}}$ and $S_{\mathrm{eff}} \to 0$) and further assumes the high-temperature limit [$\Lambda_{\mathrm{th}}(T) \to \Lambda_{\mathrm{tot}}$]. As a consequence, all intramolecular modes now contribute to the activation barrier imposed by Λ_{tot} [see Figs. 7(e) and 7(f) in Appendix B for a visualization of the resulting change in the spectra]. This overestimation of the energy barrier leads, in average, to a decrease of the hopping rate compared to mLJH. The resulting MH mobilities [Fig. 5(c)] show, on average over all hopping materials, an underestimation of the mobility compared to experimental values ($\Delta_{\mathrm{hop}} = 0.6$).

A different result for the average mobility is obtained with simulations using the MH approach without environmental disorder [Fig. 5(d)]. We find that, in the absence of environmental disorder, the mobilities of MH become surprisingly similar to the experimental mobilities for both the hopping materials ($\Delta_{\mathrm{hop}} = 1.4$) and bandlike materials. This coincidence, however, should be taken with great caution, since incoherent hopping approaches should underestimate the experimental mobility of bandlike materials. Figure 5(h)

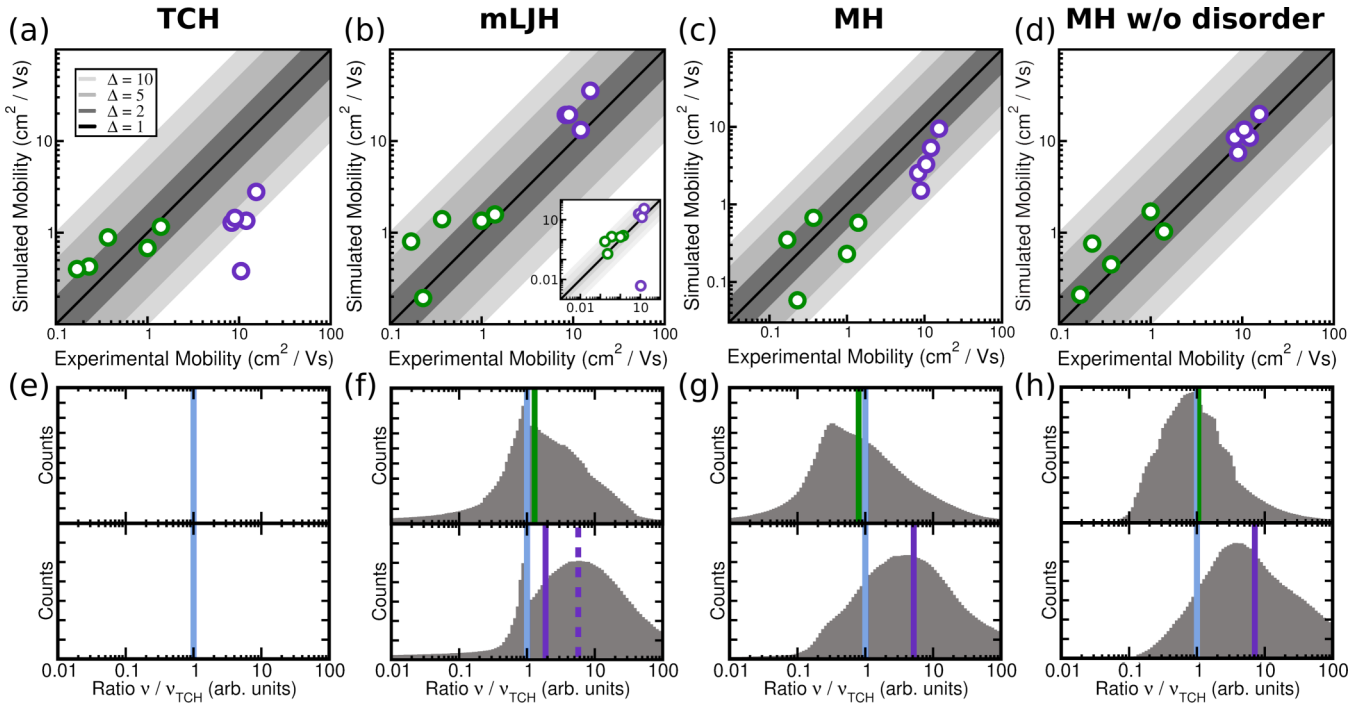

FIG. 5. (a)–(d) Comparison of different simulated hopping mobilities: (a) TCH approach with separation of dynamic and quasistatic modes; (b) mLJH approach (without TC); and (c) MH approach (without TC). The simulations in (a)–(c) include environmental contributions. (d) MH approach (without TC) and neglecting environmental contributions. Material classes are indicated as colored points: hopping (green) and bandlike (violet). The gray shaded lines in (a)–(d) indicate relative deviations between simulated and experimental mobilities. (e)–(h) Distribution of the ratios between hopping rate of the considered model and the TCH rate for hopping materials (top panel) and bandlike materials (bottom panel). The average ratios are indicated in green and violet, while the ideal ratio of one is highlighted in blue. The violet dashed in line in (f) represents the averaged ratio without pentacene.

indicates the resulting deviation from TC by up to a factor of 10, while the distribution appears more symmetric. This analysis shows that the match of MH mobilities with experimental ones likely originates from the inconsistent (dynamical and classical) treatment of the molecular vibrations in the presence of elevated hopping rates and the absence of environmental disorder.

VI. CONCLUSION

We studied a time-consistent hopping approach derived from linear-response theory, which includes both slow modes treated in the quasistatic limit and fast, dynamic modes. The time-consistent separation between both sets by the hopping time revealed that the hopping process is mediated by strongly coupling *driving modes* in accordance with other models. The resulting calculated mobilities are consistent with experimental mobilities for materials in the hopping regime. They also consistently underestimate the mobilities of a control set of bandlike materials due to missing coherent transport contributions. We further showed that other popular hopping approaches yield mobilities comparable to experimental values for all materials due to an inconsistent dynamical treatment of the intramolecular vibrations in the presence of elevated hopping rates. In these approaches, the frequent violation of time consistency is partly balanced by a cancellation of those TC errors, while the TCH approach yields consistent results for all materials under investigation. An interesting perspective for future work is the extension of the present model to nonlocal electron-phonon coupling, which requires a further generalization of the analytical derivation and the calculation of more material parameters. Although the approach was benchmarked on crystalline systems, it can equally be used to study charge transfer and transport in the large class of disordered systems and blends by including the energetics of the morphologies under study. This should pave the way to a physically more consistent description of charge carrier transport.

ACKNOWLEDGMENTS

We would like to thank the Deutsche Forschungsgemeinschaft for financial support [Projects No. OR 349/1, No. OR 349/3, and the Cluster of Excellence e-conversion (Grant No. EXC2089)]. Grants for computer time from the Zentrum für Informationsdienste und Hochleistungsrechnen of TU Dresden and the Leibniz Supercomputing Centre in Garching (SuperMUC-NG) are gratefully acknowledged.

APPENDIX A: ESTIMATION OF THE DEGREE OF LOCALIZATION

To check for the presence of localized charge carriers and classify the studied materials into the localized and delocalized transport regime, we estimate the degree of localization of the charge on a single molecule in a simple two-state model

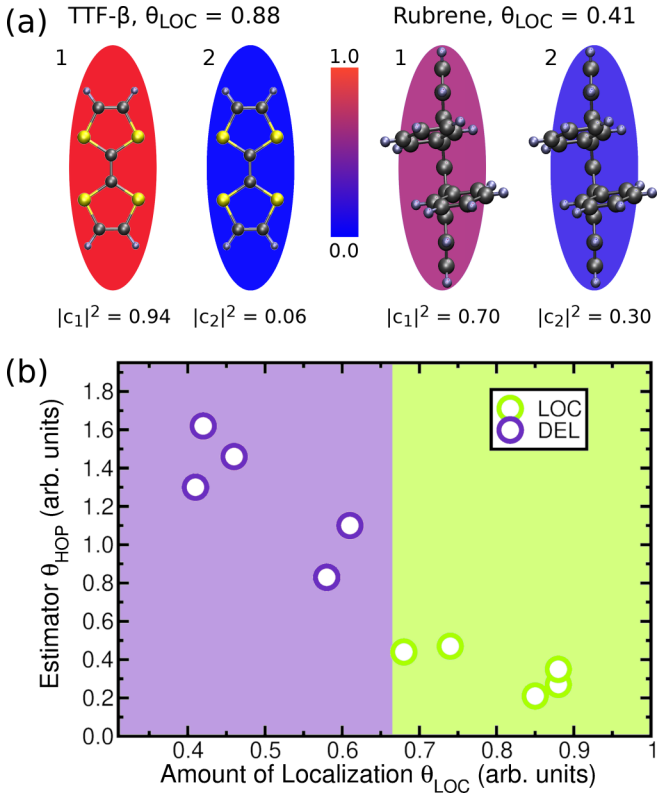

FIG. 6. Degree of localization of the charge carrier. (a) Degree of localization and the coefficients $|c_{1/2}|^2$ calculated in the two-state model for TTF-β (left) and rubrene (right). (b) Degree of localization θ_{LOC} at room temperature versus θ_{HOP} for all 10 materials studied in this work. Materials are classified into the regime of localized transport (LOC, green) and delocalized transport (DEL, violet) according to θ_{LOC}

in electronic site representation. There, a site corresponds to a particular molecular orbital of molecule 1 or 2. We therefore reduce the Holstein-Hamiltonian Eq. (2) to a purely electronic two-state Hamiltonian

$$H_{\text{two-state}} = \begin{pmatrix} 0 & \tilde{\varepsilon}_{12} \\ \tilde{\varepsilon}_{21} & (\varepsilon_2 - \varepsilon_1) \end{pmatrix}. \tag{A1}$$

In the spirit of the TCH approach, the molecular vibrations enter in Eq. (A1) in a separated fashion. The slow quasistatic modes generate disorder in the electronic on-site energies $(\varepsilon_2 - \varepsilon_1)$ following a Gaussian distribution according to Eq. (20). The fast dynamic modes generate a narrowing of the bare transfer integrals ε_{12} to $\tilde{\varepsilon}_{12}$ according to Eq. (24). In this two-state model, we chose twice the bare transfer integral $2\varepsilon_{12}$ in the hopping direction as the separating energy scale and obtain $\hbar\omega_{\mathrm{qs}} \leqslant \varepsilon_{12} < \hbar\omega_{\mathrm{dyn}}$ in analogy to Eq. (41).

The resulting eigenstates $c = (c_1, c_2)$ and $d = (d_1, d_2)$ of the two-state Hamiltonian Eq. (A1) are used for an estimation of the degree of localization θ_{LOC} caused by the vibrational disorder. In the case of vanishing electronic coupling, $\tilde{\varepsilon}_{12} = \tilde{\varepsilon}_{21} = 0$, the states are completely localized on one or the other site $|c_1|^2 = |d_2|^2 = 1.0$ and $|c_2|^2 = |d_1|^2 = 0$. In the other extreme case of vanishing disorder in the on-site energies $(\varepsilon_2 - \varepsilon_1) = 0$, the states are completely delocalized over both sites: $|c_1|^2 = |c_2|^2 = |d_1|^2 = |d_2|^2 = 0.5$. In the intermediate cases, the degree of localization depends on the ratio between $(\varepsilon_2 - \varepsilon_1)$ and $\tilde{\varepsilon}_{12}$.

We estimate the degree of localization $\theta^{\xi}_{\mathrm{LOC}}$ for a specific configuration ξ as

$$\theta^{\xi}_{\mathrm{LOC}} = 2\max(|c_1|^2, |c_2|^2) - 1, \tag{A2}$$

which is a number between 0 (complete delocalization) and 1 (complete localization). Since it is dependent on the instantaneous configuration ξ of the quasistatic modes, an ensemble average will be performed over $N = 10\,000$ different configurations to measure the averaged degree of localization:

$$\theta_{\mathrm{LOC}} = \frac{1}{N}\sum_{\xi}^{N} \theta^{\xi}_{\mathrm{LOC}}. \tag{A3}$$

The closer θ_{LOC} is to one, the higher is the localization of the charge carrier on a single site and the better is the description of the charge transfer via a hopping approach. This concept is visualized in Fig. 6(a) for the studied material with largest localization (TTF-β, $\theta_{\mathrm{LOC}} = 0.88$) and smallest degree of localization between two sites (rubrene, $\theta_{\mathrm{LOC}} = 0.41$). There the coefficients $|c_{1/2}|^2$ used to determine θ_{LOC} are presented in a color scale. For TTF-β site 1 contributes with $|c_1|^2 = 0.94$ to the new eigenstate c and thus the charge carrier can be assumed to be localized to a high degree on a single site due to the vibrational disorder and band narrowing. Thus, charge transfer will most likely take place due to dynamic changes in the disorder landscape as modeled in the TCH approach. In the case of rubrene, the sites contribute with $|c_1|^2 = 0.7$ and $|c_2|^2 = 0.3$ to the new state c. As a consequence, the charge carrier is already delocalized over the two sites due to larger transfer integrals and smaller vibrational disorder and a hopping approach based on localized charge carriers is inappropriate to model the charge transport. Since the estimation is based on *ab initio* parameters, it can also be used to check the degree of localization and expected transport mechanism for new materials that are experimentally not realized yet.

In Fig. 6(b) the estimators θ_{LOC} are visualized for all 10 materials studied in this work on the x axis (the numerical data is collected in Table I). For comparison, the commonly used estimator obtained in transition state theory [30]

$$\theta_{\mathrm{HOP}} = \frac{2\varepsilon_{MN}}{\Lambda_{\mathrm{tot}}} << 1 \tag{A4}$$

is presented on the y axis. It depends on the transfer integral in transport direction ε_{MN} and the total reorganization energy Λ_{tot} and should be smaller than one for hopping approaches to be valid. Both estimators favor the same set of materials for localized hopping transport. However, in contrast to θ_{HOP}, θ_{LOC} allows for the inclusion of environmental disorder and is temperature dependent, since it includes the thermal activation N_{λ} of the quasistatic modes. We thus use the more elaborate estimator θ_{LOC} for the classification into the localized and delocalized transport regimes. Although, realistically, there is a smooth transition between both regimes, we use a hard cut-off value for the separation, which we define as $\theta_{\mathrm{LOC}} = \frac{2}{3}$. This particular value ensures that, at room temperature, naphthalene ($\theta_{\mathrm{LOC}} = 0.68$) is included in the localized transport regime. Theoretical evidence suggests that, at room temperature, transport in naphthalene is predominantly driven by

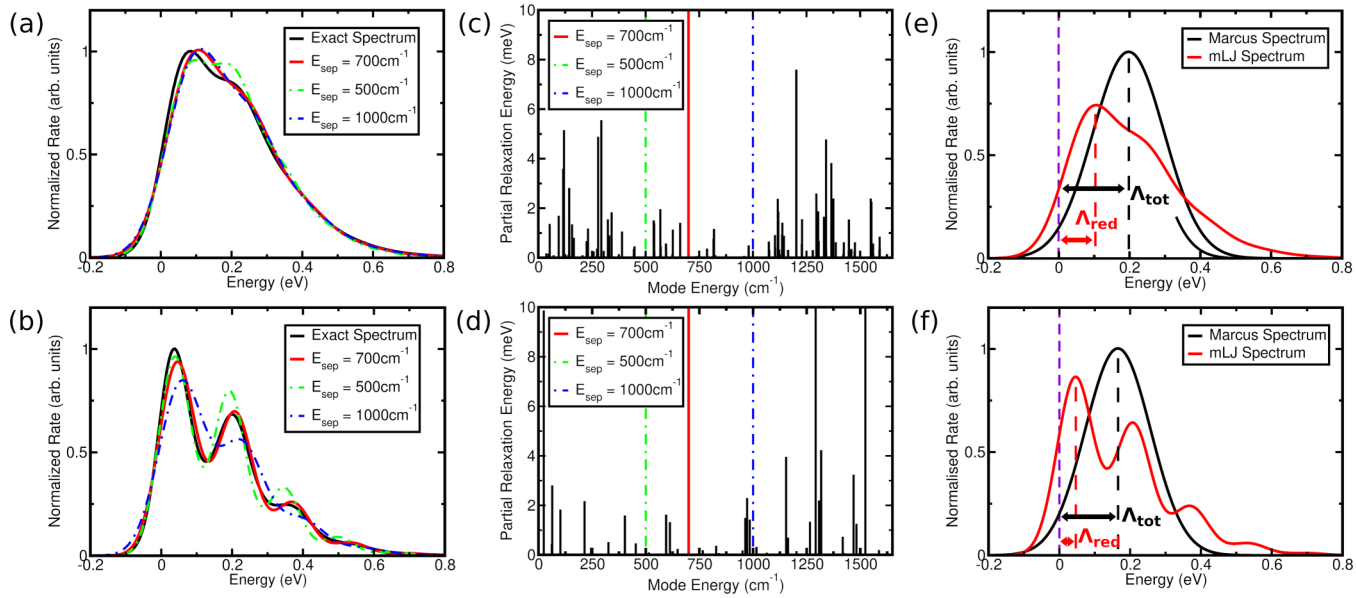

FIG. 7. Collection of the rate and vibrational spectrum for NTMTI and rubrene. Left: Comparison of the exact spectrum Eq. (B1) in black and approximated spectrum Eq. (B2) for $E_{\rm sep} = 700$ cm^{-1} in red for (a) NTMTI and (b) rubrene. The dashed lines show the approximated spectra for $E_{\rm sep} = 500$ cm^{-1} (green) and $E_{\rm sep} = 1000$ cm^{-1} (blue). Center: Vibrational mode spectrum for (c) NTMTI and (d) rubrene. The red, green, and blue bars mark the different separation energies used to compute the spectra in (a) and (b). Right: Comparison of the Marcus spectrum Eq. (B3) in black and the approximated mLJ spectrum Eq. (B2) in red for (e) NTMTI and (f) rubrene. While in Marcus theory all modes contribute to the energy barrier imposed by the reorganization energy $\Lambda_{\rm tot}$, in the mLJ approach only the low-frequency dynamic vibrations contribute to the reduced reorganization energy $\Lambda_{\rm red}$, yielding an increased hopping rate around $E \approx 0$ (violet dashed line).

incoherent transport contributions [33]. At lower temperatures, the degree of localization of naphthalene falls below the threshold value, e.g., $\theta_{\rm LOC}(100\ {\rm K}) = 0.54$ and $\theta_{\rm LOC}(20\ {\rm K}) = 0.38$. This reflects the transition to delocalized transport in naphthalene below room temperature similar to experimental and theoretical evidence [33,75].

APPENDIX B: SEPARATION OF LOW-FREQUENCY AND HIGH-FREQUENCY DYNAMIC MODES

The separation of the dynamic modes into low-frequency and high-frequency regimes is performed by means of an empirical separation energy which is found to $E_{\rm sep} = 700$ cm^{-1} as explained below. The low-frequency and high-frequency dynamic modes are defined via the existence or nonexistence of periodicity during the hopping process, as will be explained in the following. In Fig 7 the exact spectrum

$$\begin{aligned} F(\zeta) &= \int_{-\infty}^{\infty} dt e^{it\zeta/\hbar} e^{\phi^{\rm dyn}(t)}, \\ \phi^{\rm dyn}(t) &= -2\sum_{\lambda}^{\rm dyn} (g_M^{\lambda})^2 (2N_{\lambda}+1) \\ &\quad + 2\sum_{\lambda}^{\rm dyn} (g_M^{\lambda})^2 (N_{\lambda}+1) e^{-i\omega_{\lambda}t} \\ &\quad + 2\sum_{\lambda}^{\rm dyn} (g_M^{\lambda})^2 N_{\lambda} e^{i\omega_{\lambda}t}, \end{aligned} \tag{B1}$$

which is derived from the Holstein-Hamiltonian above, is presented for NTMTI [Fig. 7(a)] and rubrene [Fig. 7(b)] in black. The exact spectrum shows a phonon progression that is generated by periodic modes (high-frequency modes), whereas the broadening and shift of the particular peaks is generated by nonperiodic modes (low-frequency modes). This behavior can be qualitatively reproduced by the simpler modified Levich-Jortner spectrum also derived in the main text:

$$\begin{aligned} F(\zeta) &= \frac{\sqrt{\pi}\hbar}{\sqrt{\Lambda_{\rm th}(T) k_{\rm B} T}} e^{-S_{\rm eff}} \sum_{k=0}^{\infty} \frac{1}{k!} (S_{\rm eff})^k \\ &\quad \times \exp\left[\frac{-(\zeta - \Lambda_{\rm red} - k\hbar\omega_{\rm eff})^2}{4\Lambda_{\rm th}(T) k_{\rm B} T} \right]. \end{aligned} \tag{B2}$$

Here the high-frequency modes contribute to the phonon progression via an effective mode of energy $\hbar\omega_{\rm eff}$ and effective coupling strength $S_{\rm eff}$. The low-frequency modes contribute to the broadening by $\Lambda_{\rm th}(T) k_{\rm B} T$ and to the energy barrier by $\Lambda_{\rm red}$. The intramolecular modes can now be classified into either of these two classes for a given separation energy $E_{\rm sep}$.

The approximated spectrum Eq. (B2) is plotted in Fig. 7(a) for NTMTI and 7(b) for rubrene for different separation energies: $E_{\rm sep} = 700$ cm^{-1} (solid red), $E_{\rm sep} = 500$ cm^{-1} (dashed green), and $E_{\rm sep} = 1000$ cm^{-1} (dashed blue) and shows clear similarities to the exact spectrum. The best agreement between the exact spectrum and approximated spectrum is found for $E_{\rm sep} = 700$ cm^{-1}, which is therefore used for all materials investigated in this work. More insight into the insensitivity to the value of $E_{\rm sep}$ can be gained from the center panels in Fig. 7, which show the vibrational spectra of NTMTI in Fig. 7(c) and rubrene in Fig. 7(d). The partial relaxation energy $\Lambda_{\rm part}^{\lambda} = (g_M^{\lambda})^2 \hbar\omega_{\lambda}$ of each particular mode λ is plotted against the vibrational mode energy. In the spectra, two

regimes of strongly coupling modes can be identified: modes below 500 cm^{-1} (e.g., bending modes) and modes above 1000 cm^{-1} (e.g., stretching modes). The chosen separation energy of $E_{sep} = 700$ cm^{-1} (red bar) lies in between these two regimes and has no coupling modes in its immediate vicinity, making it suitable for the separation between low-frequency and high-frequency modes. This particular spectral shape with well separated groups of high- and low-frequency modes is typical for the organic molecules studied in this work due to structural similarities (i.e., they are all based on conjugated carbon-rich backbones). We therefore take $E_{sep} = 700$ cm^{-1} for all studied molecules.

The mLJH approach discussed in the main text is based on Eq. (B2) by treating also the quasistatic intramolecular vibrations dynamically. A further approximation to the vibrational spectrum is performed in Marcus theory, where all intramolecular vibrations are treated as low-frequency (nonperiodic) modes and the high-temperature limit $T \to \infty$ is applied. As a result, all vibrations contribute to the reorganization energy, i.e., $\hbar\omega_{eff} \to 0$ and $\Lambda_{th}(T) \to \Lambda_{red} \to \Lambda_{tot}$, which yields the spectrum

$$F(\zeta) = \frac{\sqrt{\pi}\hbar}{\sqrt{\Lambda_{tot} k_B T}} \exp\left[\frac{-(\zeta - \Lambda_{tot})^2}{4\Lambda_{tot} k_B T}\right]. \tag{B3}$$

In Figs. 7(e) and 7(f) the Marcus spectrum Eq. (B3) is shown in black and is compared to the mLJ spectrum Eq. (B2) in red for NTMTI and rubrene. Since in Marcus theory all vibrations contribute to the energy barrier Λ_{tot}, the weight of the spectrum is shifted to higher energies compared to the mLJ spectrum. This results in a decreased hopping rate around $E \approx 0$ (violet dashed line) for Marcus theory and the lower mobilities obtained compared to the mLJH approach in the main text.

APPENDIX C: COMPUTATIONAL METHODS

Molecular and crystal structures: The initial crystal structures were extracted from experimental x-ray diffraction measurements (see Table I). To specify the positions of the unresolved hydrogen atoms, a relaxation of just the hydrogen atoms was performed for every structure in small molecular clusters using DFT (Gaussian09 [85], B3LYP exchange-correlation functional [61,62], 6-311G** basis set [63,64]). Single monomers and dimers were extracted from the crystal structure to calculate the mode-resolved electron-phonon couplings, reorganization energies and transfer integrals.

Electron-phonon coupling and reorganization energies: A normal mode analysis was performed for every studied molecule in its relaxed gas phase geometry using Gaussian16 [65] (B3LYP/6-311G**). The electron-phonon coupling constants g_M^λ of each normal mode λ is calculated using the frozen-phonon approach [86]:

$$g_M^\lambda = \frac{\partial \varepsilon_M}{\partial X_\lambda} \frac{1}{\sqrt{2\omega_\lambda^3 \hbar}}, \tag{C1}$$

where ε_M is the ionization potential of the isolated monomer. With this level of precision, the computational demand for the calculation of the electron-phonon coupling is about 800 CPUh. In gas phase, the molecules TTF and DT-TTF show very large coupling constants for the low-frequency bending modes (and consequently large reorganization energies), which are not present in that extent in a crystalline environment. We therefore scale down these coupling constants such that the high-temperature limit of $\Lambda_{th}^{tot}(T)$ (including all modes) from gas phase coincides with the total reorganization energy $\Lambda_{tot}^{4\text{-point}}$ calculated with the well-established 4-point method [38] in the crystal environment. There the reorganization energy is calculated as

$$\Lambda_{tot}^{4\text{-point}} = [E_+(q_0) - E_+(q_+)] + [E_0(q_+) - E_0(q_0)]. \tag{C2}$$

$E_0(q_0)$ is the energy of the neutral molecule in its ground state and $E_0(q_+)$ is the energy of the neutral molecule in the minimum geometry of the charged state, the difference of both defines the relaxation energy of the neutral monomer. The energy difference between $E_+(q_+)$ and $E_+(q_0)$ defines the relaxation energy of the charged monomer, respectively. The crystal environment is modeled by including all nearest-neighbor molecules of the center molecule that relaxes. The atomic positions of the surrounding molecules were fixed during the relaxation runs and the charging states were ensured by using charge constraints. These calculations were performed using the NWchem [87] package and the B3LYP hybrid functional, together with the 6-311G** basis set.

Transfer integrals: The transfer integrals ε_{MN} were calculated for dimer systems according to the fragment orbital method [88]. They are obtained as the matrix element of a reference Hamiltonian $\hat{F}$ with respect to the frontier orbitals ϕ_M of the monomers:

$$\varepsilon_{MN} = \langle \phi_M | \hat{F} | \phi_N \rangle. \tag{C3}$$

Since the monomer orbitals of different molecules are in general not orthogonal, in contrast to the desirable definition of the transfer integral with orthogonal states, the reference Hamiltonian $\hat{F}$ is obtained by a Löwdin orthogonalization [89] of an original Hamiltonian F:

$$\hat{F} = S^{-1/2} F S^{-1/2}. \tag{C4}$$

The original Hamiltonian of the dimer (which is the Fock matrix F), the overlap matrix S, and the monomer orbitals were obtained by DFT calculations with the Gaussian16 package and the B3LYP level of theory combined with the 6-311G** basis set. With this configuration, the calculation of a single transfer integral requires, on average, 0.5 CPUh.

Environmental disorder: Additional environmental disorder contributions, such as intermolecular modes and polarization corrections from the surrounding molecules that can affect the charge-transfer process, were included into the calculations. In the common approach, the environmental contributions are treated as thermal disorder modeled by a Gaussian distribution of standard deviation σ_{env}, the disorder parameter [38,90]. This static disorder parameter can be converted to the dynamic temperature-dependent reorganization energy from the main text via $\sigma_{env}^2 = 2\Lambda_{th} k_B T$. The calculations of σ_{env} have been performed by Yavuz *et al.* [66] for a large amount of molecules and we take these parameters if available (see Table I). Depending on the size of the hopping rate, the environmental modes can now either contribute

dynamically in form of the additional reorganization energy $\Lambda_{\text{th}}T = \frac{\sigma_{\text{env}}^2}{2k_{\text{B}}T}$ with a typical mode energy of $\hbar\omega_{\text{env}} = 5$ meV [16], or statically by means of the disorder parameter σ_{env}. During our calculations we found that the environmental modes are so slow that the usual static treatment is valid for nearly all of the studied materials.

Charge transport simulations: Kinetic Monte Carlo simulations were performed to simulate the charge transport in finite 3D bulk systems. The TCH rates, mLJH rates, and MH rates were used as introduced in the main text. The hopping sites were chosen as the center-of-mass positions of single molecules in the experimental crystal structure. The simulations were performed with 100 000 time steps and averaged over 20 000 trajectories. This ensures that the TCH rates are averaged over multiple configurations $\boldsymbol{\xi}$ of the quasistatic modes to fulfill Eq. (14) in the main text. The computational demand for a single KMC run with 100 000 steps for an average molecule of approximately 40 atoms and 14 nearest neighbors is about 4 s on a single CPU and scales linearly with the number of seeds/disorder configurations used in the average. The anisotropic mobilities were obtained by using the Einstein-relation

$$\mu_\alpha = \frac{e_0}{k_{\text{B}}T}\frac{\langle x_\alpha^2\rangle}{2t}. \tag{C5}$$

The square-displacement x_α^2 and time t were obtained as the final position and elapsed time of each trajectory. The spatially resolved mobility is obtained by projecting the sheaf of results of all 3D trajectories onto the respective spatial directions. The final mobilities shown in the main text is the maximum obtained mobility, being closest to the maximum intrinsic mobility.

[1] S. Reineke, F. Lindner, G. Schwartz, N. Seidler, K. Walzer, B. Lüssem, and K. Leo, Nature (London) **459**, 234 (2009).
[2] B. Kippelen and J.-L. Brédas, Energy Environ. Sci. **2**, 251 (2009).
[3] H. Dong, C. Wang, and W. Hu, Chem. Commun. **46**, 5211 (2010).
[4] M. E. Gershenson, V. Podzorov, and A. F. Morpurgo, Rev. Mod. Phys. **78**, 973 (2006).
[5] J. Mei, Y. Diao, A. L. Appleton, and Z. Bao, J. Am. Chem. Soc. **135**, 6724 (2013).
[6] G. Chidichimo and L. Filippelli, Int. J. Photoenergy **2010**, 123534 (2010).
[7] W. Cao and X. Jiangeng, Energy Environ. Sci. **7**, 2123 (2014).
[8] X. Yang, G. Zhou, and W.-Y. Wong, J. Mater. Chem. C **2**, 1760 (2014).
[9] A. P. Kulkarni, C. J. Tonzola, A. Babel, and S. A. Jenekhe, Chem. Mater. **16**, 4556 (2004).
[10] L. Meng, Y. Zhang, X. Wan, C. Li, X. Zhang, Y. Wang, X. Ke, Z. Xiao, L. Ding, R. Xia, H.-L. Yip, Y. Cao, and Y. Chen, Science **361**, 1094 (2018).
[11] H. Sirringhaus, Adv. Mater. **26**, 1319 (2014).
[12] A. R. Murphy and J. M. Fréchet, Chem. Rev. **107**, 1066 (2007).
[13] K. Hannewald and P. A. Bobbert, Phys. Rev. B **69**, 075212 (2004).
[14] A. Troisi and G. Orlandi, Phys. Rev. Lett. **96**, 086601 (2006).
[15] A. Massé, P. Friederich, F. Symalla, F. Liu, R. Nitsche, R. Coehoorn, W. Wenzel, and P. A. Bobbert, Phys. Rev. B **93**, 195209 (2016).
[16] S. Fratini, S. Ciuchi, D. Mayou, G. Trambly de Laissardière, and A. Troisi, Nat. Mater. **16**, 998 (2017).
[17] C. Gaul, S. Hutsch, M. Schwarze, K. Schellhammer, F. Bussolotti, S. Kera, G. Cuniberti, K. Leo, and F. Ortmann, Nat. Mater. **17**, 439 (2018).
[18] M. Schwarze, C. Gaul, R. Scholz, F. Bussolotti, A. Hofacker, K. S. Schellhammer, B. Nell, B. D. Naab, Z. Bao, D. Spoltore, K. Vandewal, J. Widmer, S. Kera, N. Ueno, F. Ortmann, and K. Leo, Nat. Mater. **18**, 242 (2019).
[19] H. T. Yi, Y. N. Gartstein, and V. Podzorov, Sci. Rep. **6**, 23650 (2016).
[20] H. Ishii, K. Honma, N. Kobayashi, and K. Hirose, Phys. Rev. B **85**, 245206 (2012).
[21] M. C. Heiber, C. Baumbach, V. Dyakonov, and C. Deibel, Phys. Rev. Lett. **114**, 136602 (2015).
[22] S. Giannini, A. Carof, M. Ellis, H. Yang, O. G. Ziogos, S. Ghosh, and J. Blumberger, Nat. Commun. **10**, 3843 (2019).
[23] J. H. Fetherolf, D. Golež, and T. C. Berkelbach, Phys. Rev. X **10**, 021062 (2020).
[24] P. Ordejón, D. Boskovic, M. Panhans, and F. Ortmann, Phys. Rev. B **96**, 035202 (2017).
[25] A. Girlando, L. Grisanti, M. Masino, I. Bilotti, A. Brillante, R. G. Della Valle, and E. Venuti, Phys. Rev. B **82**, 035208 (2010).
[26] V. Coropceanu, J. Cornil, D. A. d. S. Filho, Y. Olivier, R. Silbey, and J.-L. Brédas, Chem. Rev. **107**, 926 (2007).
[27] F. Ortmann, K. S. Radke, A. Günther, D. Kasemann, K. Leo, and G. Cuniberti, Adv. Funct. Mater. **25**, 1933 (2015).
[28] O. Ostroverkhova, Chem. Rev. **116**, 13279 (2016).
[29] X. de Vries, P. Friederich, W. Wenzel, R. Coehoorn, and P. A. Bobbert, Phys. Rev. B **97**, 075203 (2018).
[30] H. Oberhofer, K. Reuter, and J. Blumberger, Chem. Rev. **117**, 10319 (2017).
[31] T. Holstein, Ann. Phys. **8**, 325 (1959).
[32] F. Ortmann, F. Bechstedt, and K. Hannewald, Phys. Rev. B **79**, 235206 (2009).
[33] F. Ortmann, F. Bechstedt, and K. Hannewald, New J. Phys. **12**, 023011 (2010).
[34] S. Fratini, D. Mayou, and S. Ciuchi, Adv. Funct. Mater. **26**, 2292 (2016).
[35] T. Nematiaram, S. Ciuchi, X. Xie, S. Fratini, and A. Troisi, J. Phys. Chem. C **123**, 6989 (2019).
[36] T. Nematiaram, D. Padula, A. Landi, and A. Troisi, Adv. Funct. Mater. **30**, 2001906 (2020).
[37] A. Sokolov, S. Atahan-Evrenk, R. Mondal, H. B. Akkerman, R. S. Sánchez-Carrera, S. Granados-Focil, J. Schrier, S. C. B. Mannsfeld, A. P. Zoombelt, Z. Bao, and A. Aspuru-Guzik, Nat. Commun. **2**, 437 (2011).
[38] V. Rühle, A. Lukyanov, F. May, M. Schrader, T. Vehoff, J. Kirkpatrick, B. Baumeier, and D. Andrienko, J. Chem. Theory Comput. **7**, 3335 (2011).

[39] P. Friedrich, V. Meded, A. Poschlad, T. Neumann, V. Rodin, V. Stehr, F. Symalla, D. Danilov, G. Lüdemann, R. F. Fink, I. Kondov, F. von Wrochem, and W. Wenzel, Adv. Funct. Mater. **26**, 5757 (2016).

[40] K. S. Schellhammer, T.-Y. Li, O. Zeika, C. Körner, K. Leo, F. Ortmann, and G. Cuniberti, Chem. Mater. **29**, 5525 (2017).

[41] M. D. Newton and N. Sutin, Ann. Rev. Phys. Chem. **35**, 437 (1984).

[42] H. Yang, F. Gajdos, and J. Blumberger, J. Phys. Chem. C **121**, 7689 (2017).

[43] R. A. Marcus, J. Chem. Phys. **24**, 966 (1956).

[44] R. A. Marcus and N. Sutin, Biochim. Biophys. Acta **811**, 265 (1985).

[45] K. Vandewal, J. Benduhn, K. S. Schellhammer, T. Vangerven, J. E. Rückert, F. Piersimoni, R. Scholz, O. Zeika, Y. Fan, S. Barlow, D. Neher, S. R. Marder, J. Manca, D. Spoltore, G. Cuniberti, and F. Ortmann, J. Am. Chem. Soc. **139**, 1699 (2017).

[46] A. Atxabal, T. Arnold, S. Parui, S. Hutsch, E. Zuccatti, R. Llopis, M. Cinchetti, F. Casanova, F. Ortmann, and L. E. Hueso, Nat. Commun. **10**, 2089 (2019).

[47] J. Jortner, J. Chem. Phys. **64**, 4860 (1976).

[48] G. Nan, X. Yang, L. Wang, Z. Shuai, and Y. Zhao, Phys. Rev. B **79**, 115203 (2009).

[49] D. V. Matyushov, J. Chem. Phys. **130**, 164522 (2009).

[50] J. Blumberger, Chem. Rev. **115**, 11191 (2015).

[51] R. Kubo, J. Phys. Soc. Jpn. **12**, 570 (1957).

[52] G. D. Mahan, *Many-Particle Physics*, 3rd ed. (Kluwer Academic/Plenum, New York, 2000).

[53] M. Panhans and F. Ortmann, Phys. Rev. Lett. **127**, 016601 (2021).

[54] T. Nematiaram and A. Troisi, J. Chem. Phys. **152**, 190902 (2020).

[55] G. Schweicher, G. D'Avino, M. T. Ruggiero, D. J. Harkin, K. Broch, D. Venkateshvaran, G. Liu, A. Richard, C. Ruzié, J. Armstrong, A. R. Kennedy, K. Shankland, K. Takimiya, Y. H. Geerts, J. A. Zeitler, S. Fratini, and H. Sirringhaus, Adv. Mater. **31**, 1902407 (2019).

[56] I. G. Lang and Y. A. Firsov, Sov. Phys. JETP **16**, 1301 (1963).

[57] A. Troisi and G. Orlandi, J. Phys. Chem. A **110**, 4065 (2006).

[58] A. Einstein, Ann. Phys. **322**, 549 (1905).

[59] M. von Smoluchowski, Ann. Phys. **326**, 756 (1906).

[60] N. R. Kestner, J. Logan, and J. Jortner, J. Phys. Chem. **78**, 2148 (1974).

[61] A. D. Becke, Phys. Rev. A **38**, 3098 (1988).

[62] C. Lee, W. Yang, and R. G. Parr, Phys. Rev. B **37**, 785 (1988).

[63] R. Krishnan, J. S. Binkley, R. Seeger, and J. A. Pople, J. Chem. Phys. **72**, 650 (1980).

[64] A. D. McLean and G. S. Chandler, J. Chem. Phys. **72**, 5639 (1980).

[65] M. J. Frisch, G. W. Trucks, H. B. Schlegel, G. E. Scuseria, M. A. Robb, J. R. Cheeseman, G. Scalmani, V. Barone, G. A. Petersson, H. Nakatsuji, X. Li, M. Caricato, A. V. Marenich, J. Bloino, B. G. Janesko, R. Gomperts, B. Mennucci, H. P. Hratchian, J. V. Ortiz, A. F. Izmaylov *et al.*, Gaussian16 Revision B.01 (2016).

[66] I. Yavuz, B. N. Martin, J. Park, and K. N. Houk, J. Am. Chem. Soc. **137**, 2856 (2015).

[67] A. Ellern, J. Bernstein, J. Y. Becker, S. Zamir, L. Shahal, and S. Cohen, Chem. Mater. **6**, 1378 (1994).

[68] H. Jiang, X. Yang, Z. Cui, Y. Liu, H. Li, W. Hu, Y. Liu, and D. Zhu, Appl. Phys. Lett. **91**, 123505 (2007).

[69] E. M. García-Frutos, E. Gutierrez-Puebla, M. A. Monge, R. Ramírez, P. de Andrés, A. de Andrés, R. Ramírez, and B. Gómez-Lor, Org. Electron. **10**, 643 (2009).

[70] R. Kabe, H. Nakanotani, T. Sakanoue, M. Yahiro, and C. Adachi, Adv. Mater. **21**, 4034 (2009).

[71] H. Nakanotani, M. Saito, H. Nakamura, and C. Adachi, Appl. Phys. Lett. **95**, 033308 (2009).

[72] C. Rovira, J. Veciana, N. Santalo, J. Tarres, J. Cirujeda, E. Molins, J. Llorca, and E. Espinosa, J. Org. Chem. **59**, 3307 (1994).

[73] M. Mas-Torrent, M. Durkut, P. Hadley, X. Ribas, and C. Rovira, J. Am. Chem. Soc. **126**, 984 (2004).

[74] H. C. Alt, J. Kalus, and IUCr, Acta Crystallogr. Sect. B **38**, 2595 (1982).

[75] W. Warta, R. Stehle, and N. Karl, Appl. Phys. A Solids Surfaces **36**, 163 (1985).

[76] C. Mitsui, T. Okamoto, M. Yamagishi, J. Tsurumi, K. Yoshimoto, K. Nakahara, J. Soeda, Y. Hirose, H. Sato, A. Yamano, T. Uemura, and J. Takeya, Adv. Mater. **26**, 4546 (2014).

[77] A. De, R. Ghosh, S. Roychowdhury, and P. Roychowdhury, Acta Crystallogr. Sect. C **41**, 907 (1985).

[78] Q. Xin, S. Duhm, F. Bussolotti, K. Akaike, Y. Kubozono, H. Aoki, T. Kosugi, S. Kera, and N. Ueno, Phys. Rev. Lett. **108**, 226401 (2012).

[79] T. Yamamoto and K. Takimiya, J. Am. Chem. Soc. **129**, 2224 (2007).

[80] S. Haas, Y. Takahashi, K. Takimiya, and T. Hasegawa, Appl. Phys. Lett. **95**, 022111 (2009).

[81] S. Schiefer, M. Huth, A. Dobrinevski, and B. Nickel, J. Am. Chem. Soc. **129**, 10316 (2007).

[82] J. Y. Lee, S. Roth, and Y. W. Park, Appl. Phys. Lett. **88**, 252106 (2006).

[83] O. D. Jurchescu, A. Meetsma, and T. T. M. Palstra, Acta Crystallogr. Sect. B **62**, 330 (2006).

[84] V. C. Sundar, J. Zaumseil, V. Podzorov, E. Menard, R. L. Willett, T. Someya, M. E. Gershenson, and J. A. Rogers, Science (80) **303**, 1644 (2004).

[85] M. J. Frisch, G. W. Trucks, H. B. Schlegel, G. E. Scuseria, M. A. Robb, J. R. Cheeseman, G. Scalmani, V. Barone, B. Mennucci, G. A. Petersson, H. Nakatsuji, M. Caricato, X. Li, H. P. Hratchian, A. F. Izmaylov, J. Bloino, G. Zheng, J. L. Sonnenberg, M. Hada, M. Ehara *et al.*, Gaussian 09 Revision E.01.

[86] F. Giustino, Rev. Mod. Phys. **89**, 015003 (2017).

[87] M. Valiev, E. J. Bylaska, N. Govind, K. Kowalski, T. P. Straatsma, H. J. J. Van Dam, D. Wang, J. Nieplocha, E. Apra, T. L. Windus, and W. A. de Jong, Comput. Phys. Commun **181**, 1477 (2010).

[88] B. Baumeier, J. Kirckpatrick, and D. Andrienko, Phys. Chem. Chem. Phys. **12**, 11103 (2010).

[89] P. O. Löwdin, J. Chem. Phys. **18**, 365 (1950).

[90] B. Thole, Chem. Phys. **59**, 341 (1981).